

# Understanding single-top-quark production and jets at hadron colliders

Zack Sullivan

*Theoretical Physics Department,  
Fermi National Accelerator Laboratory,  
Batavia, IL 60510-0500, USA*

(Dated: August 3, 2004)

## Abstract

I present an analysis of fully differential single-top-quark production plus jets at next-to-leading order. I describe the effects of jet definitions, top-quark mass, and higher orders on the shapes and normalizations of the kinematic distributions, and quantify all theoretical uncertainties. I explain how to interpret next-to-leading-order jet calculations, and compare them to showering event generators. Using the program ZTOP, I show that HERWIG and PYTHIA significantly underestimate both  $s$ -channel and  $t$ -channel single-top-quark production, and propose a scheme to match the relevant samples to the next-to-leading-order predictions.

PACS numbers: 14.65.Ha, 12.38.Bx, 13.85.Lg, 13.87.Ce

## I. INTRODUCTION

The discovery of single-top-quark production will be the flagship measurement of run II at the Fermilab Tevatron. Preliminary run II results [1] are already surpassing the limits set by the CDF [2] and D0 [3] Collaborations using data from run I. Over the next few years, the single-top-quark cross sections will be accurately measured at both the Fermilab Tevatron [4] and the CERN Large Hadron Collider (LHC) [5]. In order to compare the coming measurements of single-top-quark production to theory, a detailed understanding of the predictions for jet distributions, and the associated uncertainties is required.

The measurement of single-top-quark production will provide an excellent opportunity to study the charged-current weak-interaction of the top quark. Within the standard model, a measurement of the cross section allows direct extraction of the Cabibbo-Kobayashi-Maskawa (CKM) matrix element  $|V_{tb}|^2$ . In Fig. 1 we see that  $V_{tb}$  appears in the leading-order (LO) Feynman diagrams for  $t$ -channel production [6, 7, 8, 9, 10, 11, 12, 13],  $s$ -channel production [13, 14, 15, 16, 17, 18], and  $Wt$ -associated production [10, 19, 20, 21, 22]. This paper focuses on  $s$ -channel and  $t$ -channel production, which have sizable cross sections, and may be distinguished experimentally by the number of  $b$  tags in the final state [23]. Since the  $Wt$ -associated production cross section is small at the Tevatron, and no differential next-to-leading-order calculation exists,  $Wt$  production is not addressed here.

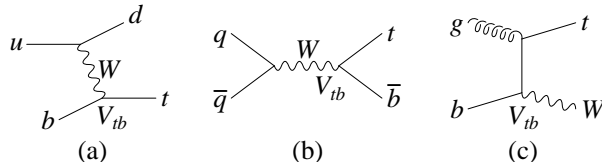


FIG. 1: Representative leading-order Feynman diagrams for (a)  $t$ -channel, (b)  $s$ -channel, and (c)  $Wt$ -associated production of a single top quark. The CKM matrix element  $V_{tb}$  appears directly in the production diagrams.

Models that extend the standard model often predict large corrections to  $s$ -channel or  $t$ -channel production, but not to both [24]. Anything that produces an anomalous coupling [24, 25, 26, 27, 28, 29, 30, 31, 32], or flavor changing neutral current [24, 33], between the top quark and any other quark opens new production modes in the  $t$ -channel, but only slightly reduces the fraction of  $b$  jets in  $s$ -channel production. Conversely, any process that allows

a new intermediate particle, such as strong dynamics [34, 35, 36, 37], a charged top-pion [24, 38, 39, 40], Kaluza-Klein modes of the  $W$  [41], or a  $W'$  boson [24, 34, 42, 43, 44], would enhance  $s$ -channel production, but is highly mass suppressed in  $t$ -channel production. In fact,  $s$ -channel single-top-quark production has been found to be the most sensitive probe of high-mass charged vector  $W'$  bosons [45] at the Tevatron [46] and LHC [47].

Both  $s$ -channel and  $t$ -channel production are important in direct searches for CP violation [48, 49, 50],  $R$ -parity-conserving supersymmetry [51], and  $R$ -parity-violating supersymmetry [52, 53, 54, 55, 56]. Both channels also contribute a significant background to all signals that include  $W + \text{jets}$  with, or without,  $b$  tags. These backgrounds appear in a number of Higgs search channels [57] and other new physics, such as  $R$ -parity-conserving [58] and  $R$ -parity-violating [59] supersymmetry searches.

The analytic form of the fully differential next-to-leading-order (NLO) cross section for  $s$ -channel and  $t$ -channel production of a single top-quark plus one jet appears in Ref. [13]. The spin-averaged version of that calculation is available from this author in the form of a FORTRAN program called ZTOP, and is used in this paper. A recurring theme throughout the analysis of the kinematic distributions is that the next-to-leading-order calculation describes *jets*, and not partons. This affects the questions that may be asked about the final state, and contributes additional challenges to the matching between theory and experiment.

The ultimate goal of performing differential calculations at next-to-leading order is to improve the quantitative connection between theory and experiment. As important as the distributions themselves, is a reliable estimate of the uncertainties in these distributions. Previous estimates of the uncertainties in the parton luminosities and kinematics [23] have been somewhat rough, and are revisited with more careful analysis. Analytic calculations are not typically compared to raw data, but rather to event generators, such as HERWIG [60] and PYTHIA [61], that have been tuned to fit the data. It is vital to determine whether these event generators at least predict the shapes of the measured distributions accurately. We will see that the current event generators provide very poor predictions of both  $s$ -channel and  $t$ -channel production.

This paper is organized as follows. A general search strategy for discovering single-top-quark production appears in Sec. I A. This lays the groundwork for discussing the event rates in terms of the number of jets in the final state. The next-to-leading-order distributions for both  $s$ -channel and  $t$ -channel single-top-quark production at the Tevatron are presented

in Sec. II. The hazards of treating NLO calculations as parton calculations are explored, and subtleties in the interpretation of jet calculations are discussed in detail. The bottom-quark mass is shown to have no measurable effect on the distributions. All uncertainties in the inclusive and exclusive theoretical calculations are described in Sec. III. In Sec. IV the PYTHIA [61] and HERWIG [60] event generators are shown to have poor representations of the measurable kinematic distributions. In Sec. IV C a simple scheme is proposed to match the event generators to the next-to-leading-order calculation. The paper concludes in Sec. V with a few directions for improvement.

### A. Strategy for discovery

The final state for both  $s$ - and  $t$ -channel production of single top quarks contains two jets plus the decay of a  $W$  boson. In order to extract the signal from the backgrounds, the decay of the  $W$  to an electron or muon, and a neutrino is used. The most serious background for single-top-quark production is the production of  $t\bar{t}$  pairs [23]. The number of  $t\bar{t}$  pairs that will be reconstructed in detectors at the Tevatron is about 5 times the total number of single-top-quark events in the 1  $b$ -tag sample, and about 10 times the number in the 2  $b$ -tag sample. Because there is already a top quark in the final state, the essence of any study will be to reduce the  $t\bar{t}$  background, while maintaining a measurable signal.

The most effective method to discover single-top-quark production uses a “jet veto,” which was first proposed in Ref. [23]. This method relies on the observation that in  $t\bar{t}$  production, the extra top quark tends to produce additional high- $E_T$  objects (leptons or jets) in the final state. The basic strategy is to form a sample of two jets, a lepton, and missing transverse energy  $E_T$ . If there are any additional isolated “hard” jets or leptons then the event is rejected. The term “hard” can be loosely defined to refer to any jet or lepton with  $E_T > 15\text{--}25$  GeV, and  $|\eta| < 2.5\text{--}4$ . Experimentally, the “jet veto” is identical to separating the final states into a  $W + 2$  jet exclusive sample and a  $W + 3$  jet inclusive sample.

We observe in Fig. 2 of Ref. [23] that placing cuts anywhere in the region of  $E_{Tj} = 15\text{--}25$  GeV for every jet yields the same significance. The reason is that acceptance for events that contain an extra radiated jet in the signal increases as the cut is lowered (thereby failing to pass the cuts) at the same rate that the acceptance for the highest- $E_T$  jet increases. Hence,

in order to avoid a sharp drop in efficiency, the jet veto should be set at the same  $E_T$  as the cut on the second-highest- $E_T$  jet.

The largest remaining background is  $Wjj$  production — dominantly  $Wcj + Wjj$  in the 1  $b$ -tag sample, and  $Wb\bar{b}$  in the 2  $b$ -tag sample. This background decreases as a function of reconstructed top-quark mass. Hence, a top-quark mass cut reduces this to an acceptable level. If a top-quark mass cut cannot be used, e.g., because of poor jet-energy resolution, other discriminates will have to be found. However, these will be ineffective without the corrections described in Sec. IV.

The detection strategies of Refs. [4, 23] should be merged into a program of three successive measurements. The first stage measures the  $W + 2$  jet signal with at least 1  $b$  tag. This sums over all single-top-quark production modes, and requires the least amount of integrated luminosity for discovery. As data is accumulated, the samples can be split into independent subsets with 1 or 2  $b$  tags. The 1  $b$ -tag sample can be used to study  $t$ -channel production, and the 2  $b$ -tag sample can be used to study  $s$ -channel production.

## II. NEXT-TO-LEADING-ORDER DISTRIBUTIONS

Fully differential next-to-leading-order cross sections predict *jet* distributions; they do not predict *parton* distributions. The consequences of this can be subtle, and require care when comparing fixed-order calculations with data, or with showering event generators. To understand these comparisons, only distributions for top-quark production at the Tevatron are examined. Distributions for antitop-quark production at the Tevatron differ solely by the signs of the pseudorapidities, and figures would be redundant. Since the physics issues are identical, no jet distributions for the LHC are shown.

The challenge of calculating differential cross sections is in how to deal with final-state infrared singularities. Different methods have different solutions in detail, but they all impose one of two conditions: include a jet definition, or include a hadronization function. The first consequence of including a jet definition in the base theoretical calculation is that the same choice of jet definition must be used in any comparison to data. This may appear obvious, but it contains a subtlety: how do you compare a jet that consists of a few partons with one that contains multiple particles? In Sec. IIC we will see the effect of the choice of jet definition on theoretical distributions. Comparisons between theory and experiment

are actually made at the event generator level, rather than directly with data. Hence, in Sec. IV we will adopt an effective solution for matching the NLO calculations to the event generators.

Before presenting NLO distributions, we must first understand which distributions are appropriate to calculate. We might be tempted to look at the LO diagrams and ask for the corresponding NLO distributions, but this would not be useful in general. Consider the LO diagram for  $t$ -channel production in Fig. 1(a). If we plot the NLO transverse momentum of the jet that includes the final-state  $d$  quark, we see in Fig. 2 that the calculation is not very stable. The massive dipole formalism (MDF) and phase space slicing (PSS) calculations of Ref. [13] provide the same results at the same scale. The methods only differ in the bin that exactly includes  $p_{Td} = 0$  GeV, which is an artifact of the different subtractions methods, and in any case not observable.

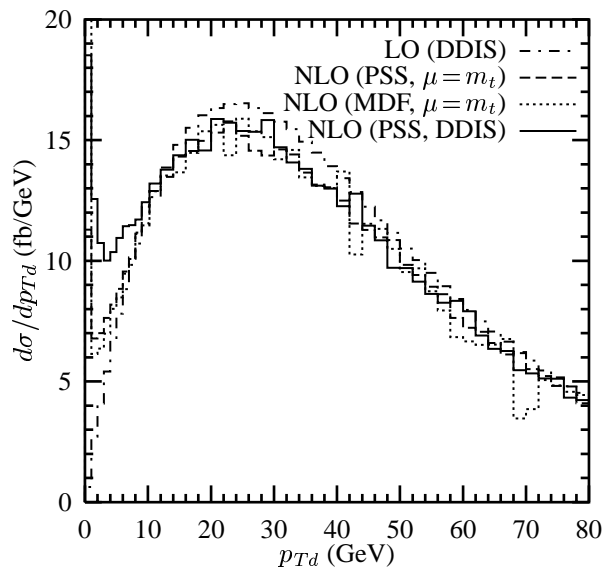


FIG. 2: Transverse momentum  $p_{Td}$  of the “ $d$ ”-jet in  $t$ -channel production at leading and next-to-leading order for the phase space slicing (PSS) and massive dipole formalism (MDF) calculations, and two scales,  $m_t$  and the double deep-inelastic-scattering scales ( $Q^2$  and  $Q^2 + m_t^2$ ). Leading order includes a  $K$ -factor of 1.09.

The problem with Fig. 2 is that the shapes of the distributions are not stable compared to scale variation or perturbative order. At leading order the  $d$  quark recoils against the massive top quark, and so has a finite distribution at small  $p_{Td}$ . At NLO the distribution takes an arbitrary value that depends on the choice of scale. Also the shapes at larger (i.e.

measurable)  $p_{Td}$  change between orders, which leads to the false impression that the NLO jets are softer than the LO parton. This figure demonstrates the danger of interpreting *jet* results in *partonic* language.

The distribution that should have been plotted is the transverse momentum of the highest- $p_T$  jet. In Fig. 3 we see that this distribution is stable in shape at different orders in perturbation theory, and for different scales. In fact the difference between the LO and NLO distribution is smaller than the NLO scale uncertainty. We also see that the choice of scale effects only normalization. Hence, we have a very well-predicted quantity.

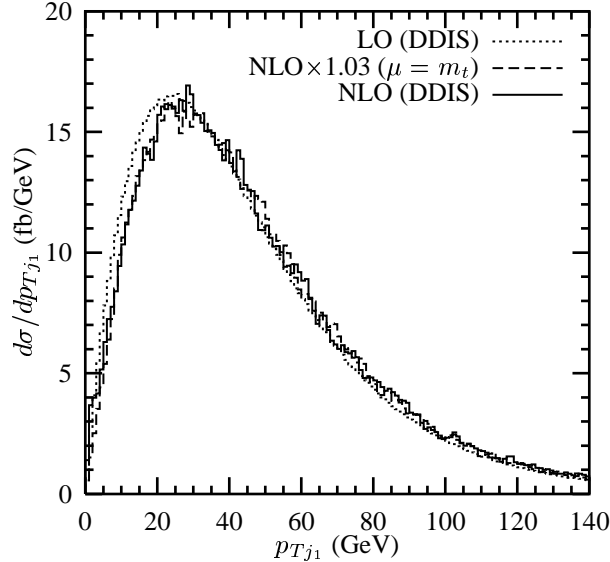


FIG. 3: Transverse momentum  $p_{T,j_1}$  of the highest- $p_T$  jet in  $t$ -channel production at leading and next-to-leading order for different scales.

What stabilizes the  $p_T$ -ordered jet at NLO if the “ $d$ ” jet is so unstable? The answer is that when the  $d$  quark becomes softer, the parton that recoils against the top quark is a  $\bar{u}$  that came from initial-state splitting of a gluon. Hence, the kinematically stable jet has a different flavor content than the LO jet. We are fortunate that we cannot distinguish experimentally the difference between a jet that started from an up or down quark. If the jet is produced with a charm or bottom quark, however, we have to track it explicitly because it might be taggable. In the case of  $t$ -channel single-top-quark production, this is CKM-suppressed and occurs less than 1% of the time in the light-quark initiated side of the diagram. Once we look at  $p_T$ -ordered jets, we will have to keep track of how often the leading jet includes a  $b$  quark from the other incoming hadron. This will not cause any stability

problems, however, since there are no overlapping singularities between the light-quark and heavy-quark initiated parts of the diagrams.

### A. $t$ -channel NLO distributions

We have seen the stability of the distribution of the highest- $p_T$  jet between leading and next-to-leading order. There are two historically relevant questions. First, how well are the leading jet and top quark distributions modeled by  $qb \rightarrow tq'$  [Fig. 4(a)] or  $qg \rightarrow t\bar{b}q'$  [Fig. 4(b)] parton-level calculations? Second, how do typical cuts effect the distributions of the top quark and jets? The analysis of leading-order  $qb \rightarrow tq'$  production plus showering is postponed until Sec. IV, when we observe the failure of the current event generators to reproduce the jet spectrum.

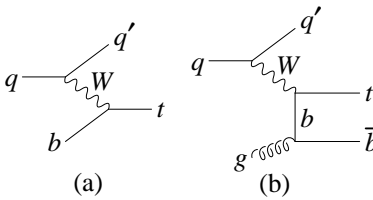


FIG. 4: Representative leading-order Feynman diagrams for (a)  $t$ -channel production ( $qb \rightarrow tq'$ ), and (b)  $W$ -gluon fusion ( $qg \rightarrow t\bar{b}q'$ ).

The analytic form of the  $t$ -channel cross section has the same form as double deep-inelastic-scattering (DDIS) [12, 13]. Color conservation enforces a natural factorization of the scales. The fermion line in Fig. 4(a) that does not include a top quark probes a proton with the DIS scale  $Q^2$ , which is identical to the virtuality of the  $W$  boson through NLO. The fermion line that does connect to a top quark sees the DIS scale for massive quarks of  $Q^2 + m_t^2$ . Another reasonable choice for both scales is the mass of the top quark. The difference between using the DDIS scales, or the top-quark mass is less than 3% at next-to-leading order. But the cross section and distributions do not change from LO to NLO when the DDIS scales are used. This is an indication of the relation of this calculation to the extraction of parton distribution functions, and DIS in general.

Even though the leading-order diagram for  $t$ -channel single-top-quark production was known to include a  $b$  quark in the initial state, the process was modeled by using the  $t\bar{b}j$  diagram shown in Fig. 4(b) at leading order in Refs. [23, 62]. To the extent that the analytic



form of the cross section is expected to look like double deep-inelastic-scattering [12, 13], this diagram was expected to give a reasonable approximation of the shape of the NLO top-quark distributions. Indeed, the  $p_{Tt}$  and pseudorapidity  $\eta_t$  distributions of the top quark are well modeled by the LO  $t\bar{b}j$  calculation. These distributions for  $t$  production at the Tevatron (a 1.96 TeV  $p\bar{p}$  collider) are shown in Figs. 5 and 6.

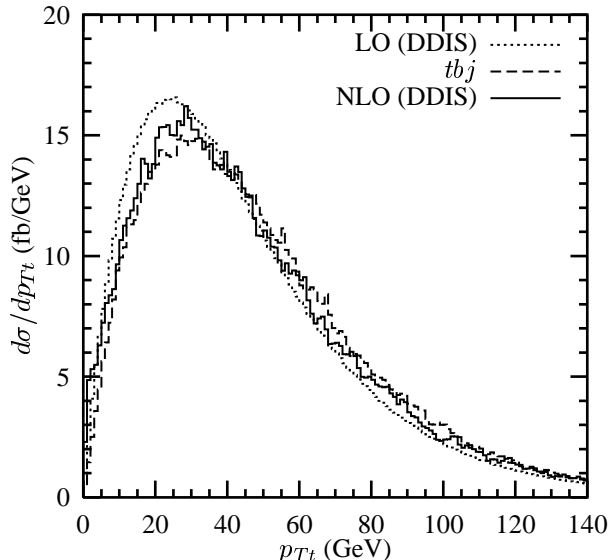


FIG. 5: Transverse momentum of the top quark  $p_{Tt}$  at LO, NLO, and from the diagram  $t\bar{b}j$ , all normalized to the  $t$ -channel NLO cross section.

The diagram  $t\bar{b}j$  should have no visible effect on the distributions of the highest- $p_T$  jet. In Figs. 7 and 8 we see that there is no difference between the true LO distributions, and the one obtained from  $t\bar{b}j$  alone. This is an additional confirmation that there is a real separation of physics between the  $Wtq$  vertex, and the vertex with no top quark. While this is a nice confirmation of the double-DIS interpretation, this means that the distributions for the highest- $p_T$  jet are more central, and slightly harder than indicated by the old approximation. Hence analyses, like that in Ref. [23] slightly underestimated the true signal.

Finally, let us examine the jet distributions as a first step in understanding the necessity of the next-to-leading-order calculations. In particular, we focus on the distributions that will be required for Sec. IV. The simple cuts in Table I separate the signal into two subsamples:  $t+1$  jet exclusive ( $Wjj$  in the experiments, or the “jet veto” of Ref. [23]), and  $t+2$  jet inclusive ( $Wjjj$  in the experiments). Jets are clustered with a  $k_T$  algorithm using  $\Delta R_{k_T} < 1.0$  (similar to a fixed cone of 0.7) and are observed if they have  $p_{Tj} > 15$  GeV and  $|\eta_j| < 2.5$ . No cuts

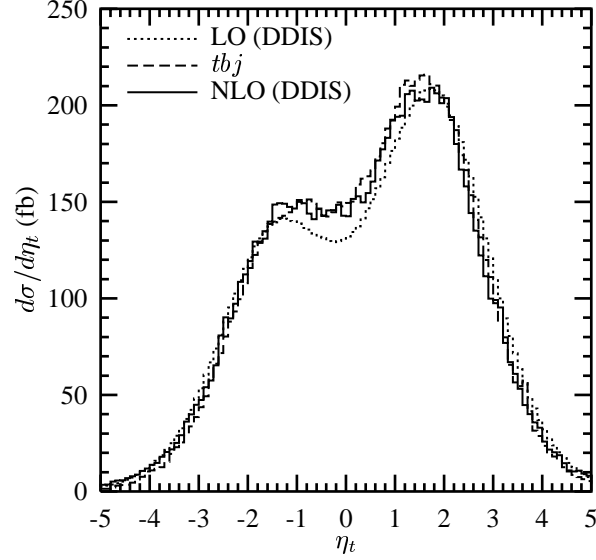


FIG. 6: Pseudorapidity of the top quark  $\eta_t$  at LO, NLO, and from the diagram  $tbj$ , all normalized to the  $t$ -channel NLO cross section.

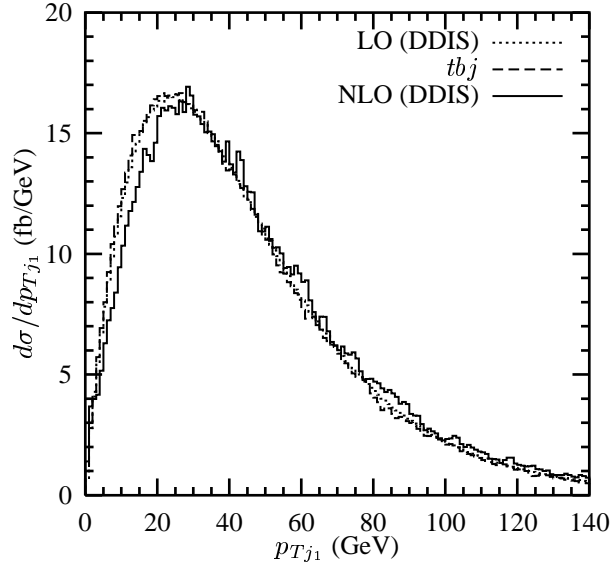


FIG. 7: Transverse momentum of the highest- $p_T$  jet  $p_{T,j_1}$  at LO, NLO, and from the diagram  $tbj$ , all normalized to the  $t$ -channel NLO cross section.

are placed on the top quark since its decay is not modeled.

In Figs. 9 and 10 we see the transverse momentum and pseudorapidity distributions for the NLO jet in the  $t + 1$  jet final state, distinguished by whether there is a  $b$  inside the jet. The distinction must be made, because the jet containing a  $b$  is both potentially taggable, and has a significantly different shape in the distributions. Notice that non- $b$  jets exhibit a

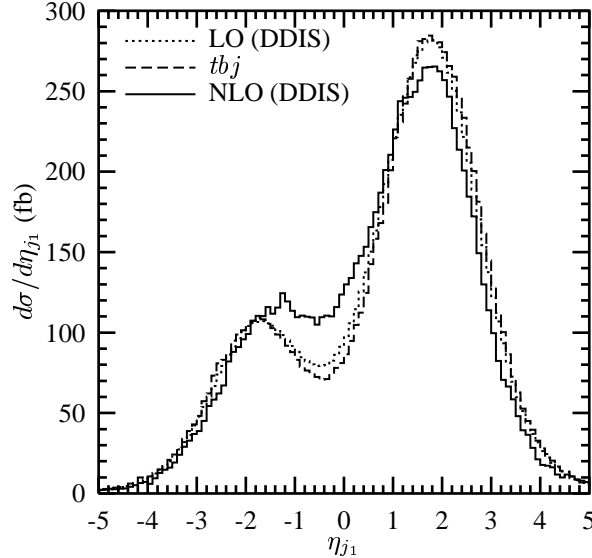


FIG. 8: Pseudorapidity of the highest- $p_T$  jet  $\eta_{j_1}$  at LO, NLO, and from the diagram  $tbj$ , all normalized to the  $t$ -channel NLO cross section.

TABLE I: Cuts on the  $p_T$ -ordered jets that define each signal region for comparison at the Tevatron. No cuts are placed on the top quark since it is not decayed.

$ \Delta R_{k_T}  < 1.0$ ( $\approx  \Delta R_{\text{cone}}  < 0.74$ )
$p_{Tj} > 15 \text{ GeV}$ , $ \eta_j  < 2.5$
$Wjj \equiv t + 1 \text{ jet ("jet veto")}$
$Wjjj \equiv t + 2 \text{ jets inclusive}$

double-peak structure, sometimes referred to as a “forward” jet. Whereas, the additional  $b$  jets tend to be very central.

In Figs. 11, 12, 13, and 14 we see the distributions for jets in the  $t + 2$  jet final state. The distinction between  $t$  plus one and two jet samples is strongly dependent on the cuts. Just as in the case of the one jet sample, the  $b$  jets are significantly more central. However, they actually peak in the opposite hemisphere from the non- $b$  jets. Approximating the additional radiation with just a  $b$  jet, as in  $t\bar{b}j$ , greatly exaggerates the centrality of the events. Hence, the only way to correctly model the signal is to include all production diagrams in a complete next-to-leading-order calculation.

In theoretical studies that used the  $t\bar{b}j$  diagram to approximate the final state, all additional radiation was implicitly assumed to come from an extra  $b$  jet. However, the NLO

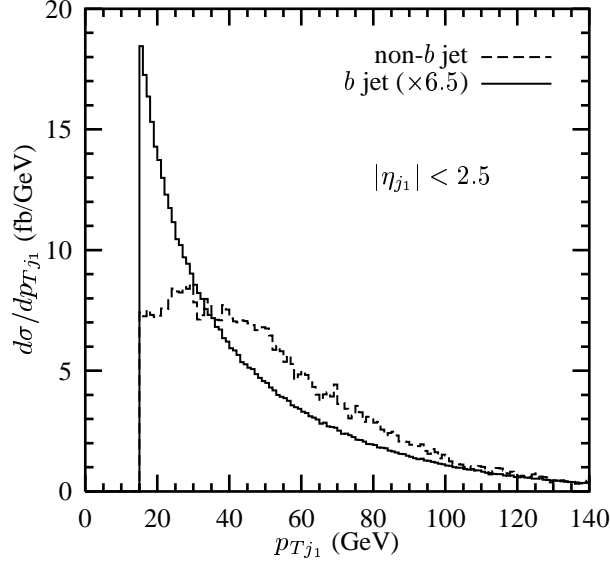


FIG. 9: Transverse momentum of the highest- $p_T$  jet  $p_{T,j_1}$  in  $t$ -channel production when it contains a  $b$ , normalized to the rate for when it is a non- $b$  jet in the  $tj$  final state.

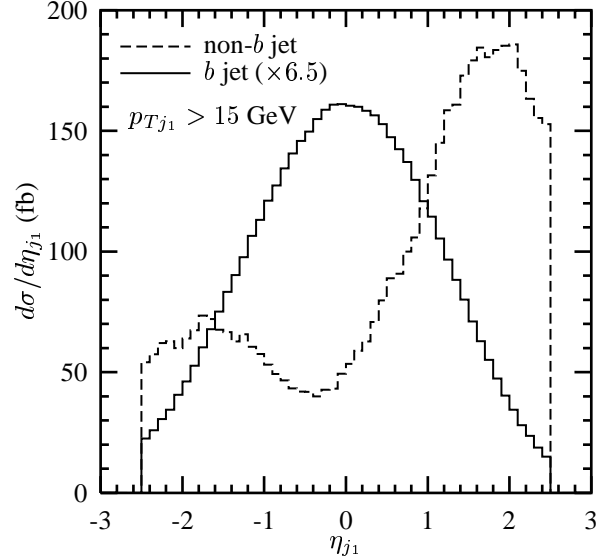


FIG. 10: Pseudorapidity of the highest- $p_T$  jet  $\eta_{j_1}$  in  $t$ -channel production when it contains a  $b$ , normalized to the rate for when it is a non- $b$  jet in the  $tj$  final state.

calculation tells us that only about 2/3 of the additional radiation includes a  $b$  jet. Fig. 10 demonstrates that the contamination from additional  $b$  jets in the  $tj$  signal is highly dependent on the choice of cuts. For the loose cuts shown, about 15% of the events have an extra  $b$  jet, but tighter cuts on the pseudorapidity will greatly enhance the relative contribution

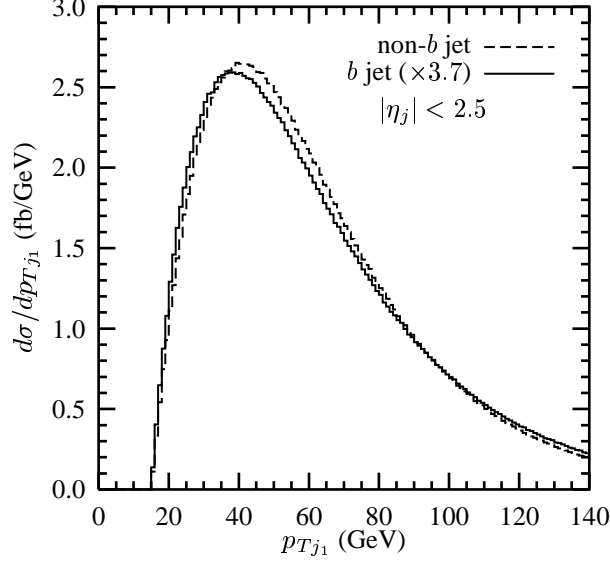


FIG. 11: Transverse momentum of the highest- $p_T$  jet  $p_{T,j_1}$  in  $t$ -channel production when it contains a  $b$ , normalized to the rate for when it is a non- $b$  jet in the  $tjj$  final state.

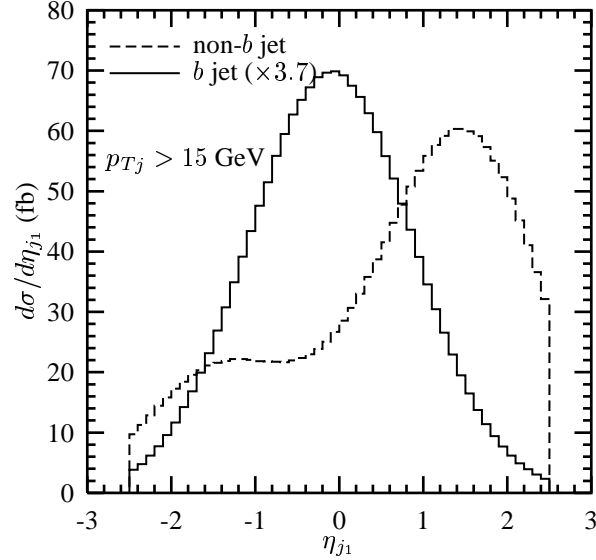


FIG. 12: Pseudorapidity of the highest- $p_T$  jet  $\eta_{j_1}$  in  $t$ -channel production when it contains a  $b$ , normalized to the rate for when it is a non- $b$  jet in the  $tjj$  final state.

from events with an extra  $b$  jet.

The next-to-leading-order calculation is necessary to properly account for the absolute cross section in each of the four final states:  $tj$ ,  $tb$ ,  $tjj$ , and  $tbj$ . In Table II we see the contribution to each final state for the simple cuts given in Table I. The  $b$  jet is the highest-

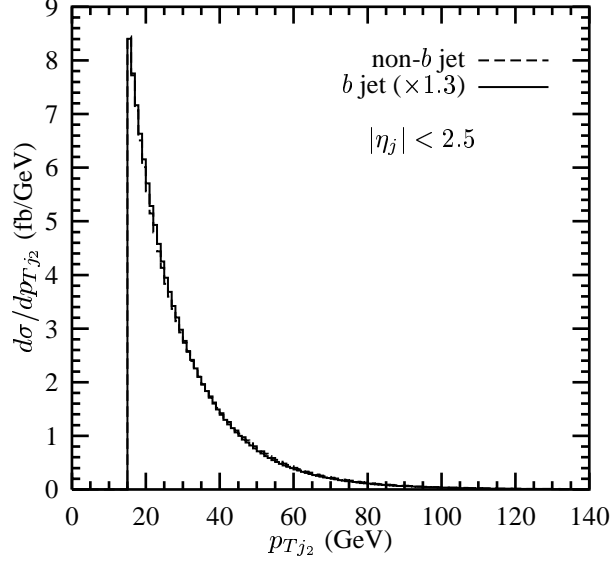


FIG. 13: Transverse momentum of the second highest- $p_T$  jet  $p_{Tj_2}$  in  $t$ -channel production when it contains a  $b$ , normalized to the rate for when it is a non- $b$  jet in the  $tjj$  final state.

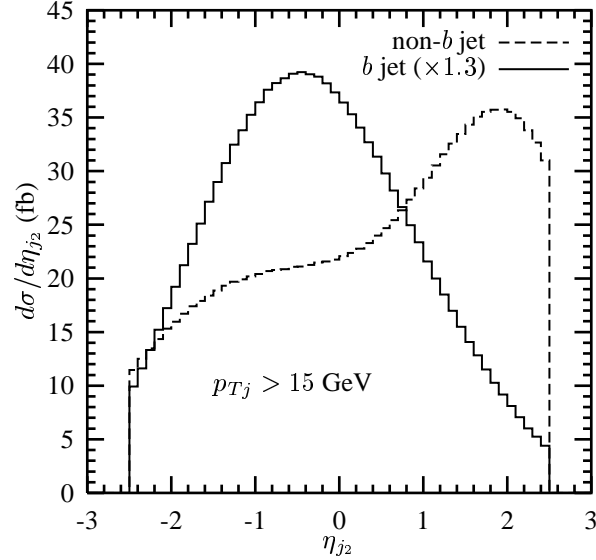


FIG. 14: Pseudorapidity of the second highest- $p_T$  jet  $\eta_{j_2}$  in  $t$ -channel production when it contains a  $b$ , normalized to the rate for when it is a non- $b$  jet in the  $tjj$  final state.

$p_T$  jet in 1/3 of the events in the  $tbj$  final state. The relative cross sections are completely insensitive to modest cuts on the top quark itself. However, it bears repeating that the percentages will change drastically if the cuts on the jets are changed. Hence, a careful matching of the NLO calculation for each choice of cuts is essential to the proper modeling

of these events.

TABLE II:  $t$ -channel and  $s$ -channel cross sections (pb) for  $t$  (or  $\bar{t}$ ) production at a 1.96 TeV  $p\bar{p}$  collider, and relative percentages of  $b$  jets vs. non- $b$  jets  $j$  in the  $t + 1$  jet exclusive and  $t + 2$  jet inclusive final states. These numbers are only valid for the cuts given in Table I. Tighter cuts on pseudorapidity typically increase the percentage of  $b$  jets in the  $t$ -channel final states.

$t$ -channel	$tj$	0.475 pb (87%)	$tjj$	0.076 pb (35%)
	$tb$	0.073 pb (13%)	$tbj$	0.139 pb (65%)
$s$ -channel	$tb$	0.310 pb (97%)	$tbj$	0.084 pb
	$tj$	0.011 pb (3%)		

### B. $s$ -channel NLO distributions

Production of a single top quark through an  $s$ -channel  $W$  boson looks very much like Drell-Yan production [13, 14, 15, 16, 63]. In Figs. 15, 16, 17, and 18 we see the transverse momentum  $p_T$  and pseudorapidity  $\eta$  of the top quark and  $\bar{b}$  jet. The large mass of the top quark protects the distributions from changing shape at next-to-leading order. Hence, it is an excellent approximation to use leading-order distributions and a  $K$ -factor of 1.54 as long as we restrict our attention to the  $t\bar{b}$  ( $Wb\bar{b}$ ) final state.

Contributions to the  $tj$  and  $tbj$  final states arise only at next-to-leading order, and will contribute a small correction to the total cross section. In Table II we see that the  $tj$  channel only contributes 3% to the  $t + 1$  jet final state, and that the ratio between the  $t + 1$  jet and  $t + 2$  jet final states is about 4 to 1. The separation between the final states is discussed in detail in Sec. IV B, where we see how the event generators fare at reproducing the jet distributions.

### C. Effect of jet definitions

Because next-to-leading-order calculations are jet calculations, and not parton calculations, results are completely dependent on the choice of jet definition. This means that no prediction is meaningful outside of the context of the particular jet definition used. Histor-

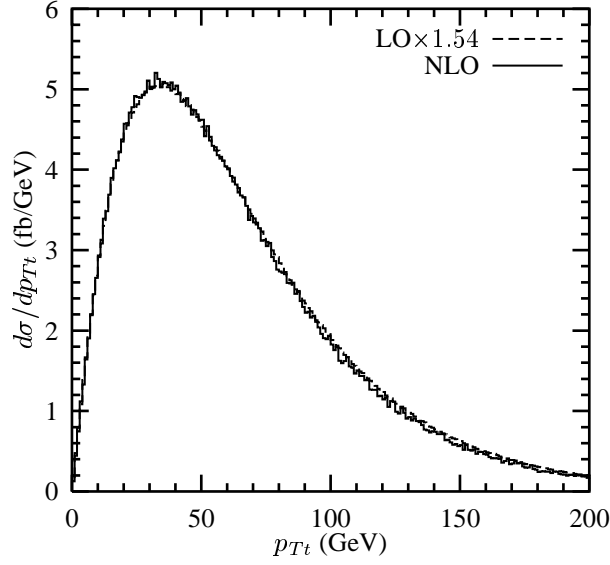


FIG. 15: Transverse momentum of the top quark  $p_{Tt}$  in  $s$ -channel production at NLO, and LO times a  $K$ -factor of 1.54.

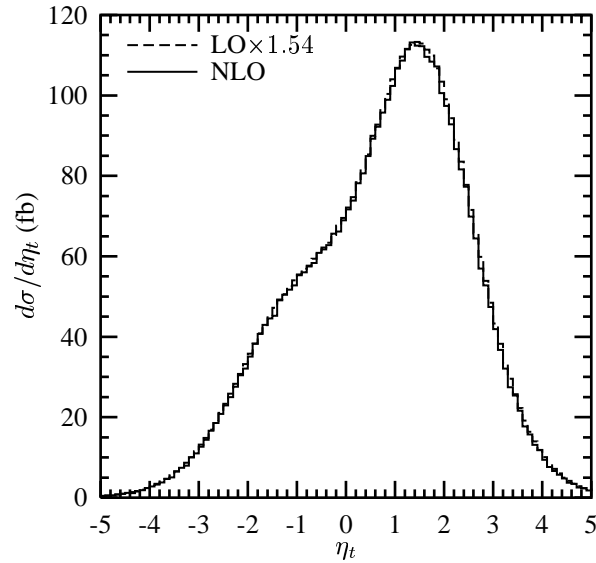


FIG. 16: Pseudorapidity of the top quark  $\eta_t$  in  $s$ -channel production at NLO, and LO times a  $K$ -factor of 1.54.

ically, jets have been discussed using fixed cones of size  $\Delta R_{\text{cone}} < 0.7$ , where  $\Delta R_{\text{cone}}$  is the distance between particles in the pseudorapidity  $\eta$ -azimuthal angle  $\phi$  plane. This definition suffers from an infrared instability, because the number of jets can change as particles fluctuate across the fixed boundary. One infrared safe [64] definition is to choose an algorithm that adaptively combines subjects as a function of their relative transverse momenta  $k_T$ . For



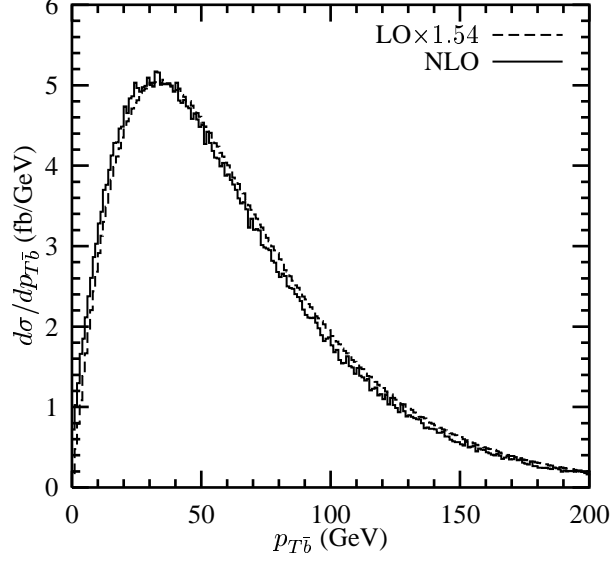


FIG. 17: Transverse momentum of the  $\bar{b}$ -jet  $p_{T\bar{b}}$  in  $s$ -channel production at NLO, and LO times a  $K$ -factor of 1.54.

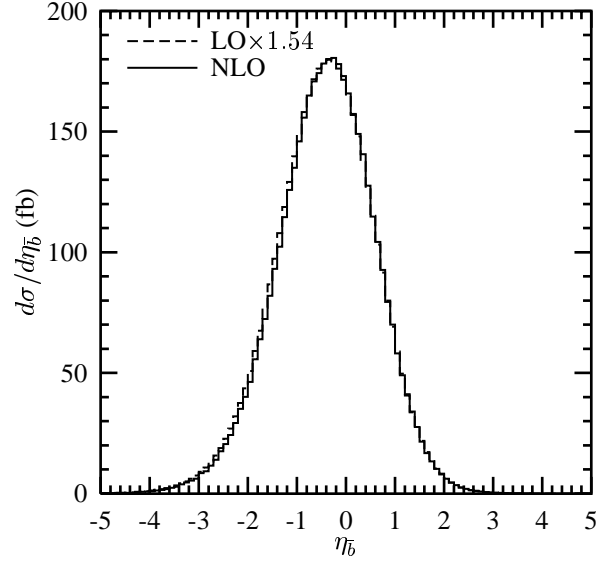


FIG. 18: Pseudorapidity of the  $\bar{b}$ -jet  $\eta_{\bar{b}}$  in  $s$ -channel production at NLO, and LO times a  $K$ -factor of 1.54.

this study the  $k_T$  cluster algorithm is used with a merging parameter  $\Delta R_{k_T} < 1.0$ , because it produces jets that are very similar to those found when using a fixed-cone of size 0.7.

In principle, the same jet definition must be used for both the theory and the experimental analyses. In practice, the NLO calculation will be matched to an event generator that is tuned to the experimental data. The NLO distributions are valid only under the jet definition

used to create them. If the experiment decides to use smaller cones, e.g., a cone of size  $\Delta R < 0.4$  is currently popular for top physics, the NLO calculation must be reevaluated. In Fig. 19 we see the ratio of the distributions  $p_{Tj_1}(\Delta R)$  over  $p_{Tj_1}(0.7)$ , where  $j_1$  is the highest- $p_T$  jet in  $t$ -channel production, and approximate fixed-cone units label the curves (the actual  $\Delta R_{k_T}$  used are larger by a factor of 1.35). We see there is a 10% change in the slope of the distribution between different typical cone sizes (0.4, 1.0) and the standard cone size 0.7. A mismatch between the cone size in the theory calculation and experimental calculation could lead to a larger error than all theoretical uncertainties combined.

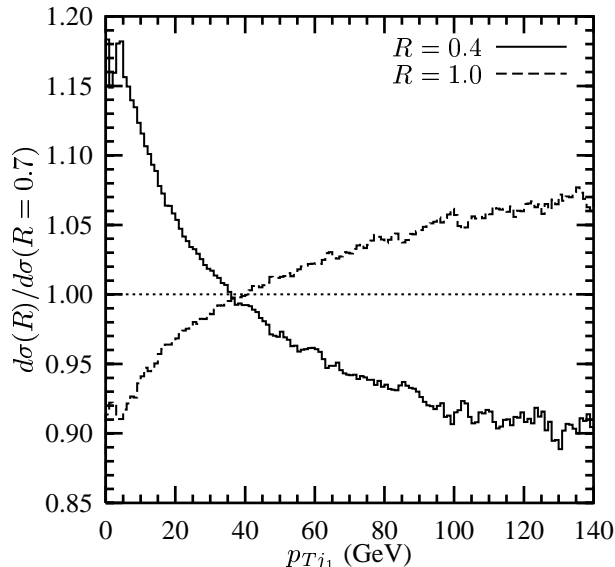


FIG. 19: Ratio  $d\sigma(R)/dp_{Tj_1}$  to  $d\sigma(R = 0.7)/dp_{Tj_1}$  for the highest- $p_T$  jet in  $t$ -channel production.

When cuts are made on the leading jet, they are typically made between 15–25 GeV. From Fig. 7 we see that this is close to the peak of the transverse momentum distribution. The jets that are measured have a falling  $p_T$  spectrum. Hence, Fig. 19 suggests that it is advisable to use the largest jet size possible. This would reduce jet-energy corrections for out-of-cone effects, and increase the signal acceptance, while having little effect on the  $Wjj$  backgrounds. The  $t\bar{t}$  background will increase slightly, but is not expected to overcome the increased signal.

### D. Effect of bottom-quark mass

When there is an additional bottom quark in the  $t$ -channel cross section, we might be concerned whether its mass is relevant to the calculation. The same almost-collinear singularity that must be resummed in the inclusive cross section appears in the distribution of this additional jet at low transverse momentum. In Fig. 20 we see the transverse energy of the extra bottom jet  $E_{T\bar{b}}$  with no cuts, compared to distribution from leading-order  $t\bar{b}j$  with a finite  $b$  mass. The curves are very similar ( $< 10\%$ ) above 10 GeV and differ by only a few percent by 15 GeV. This confirms the standard belief that a massive particle behaves the same as a massless particle in the large momentum limit.

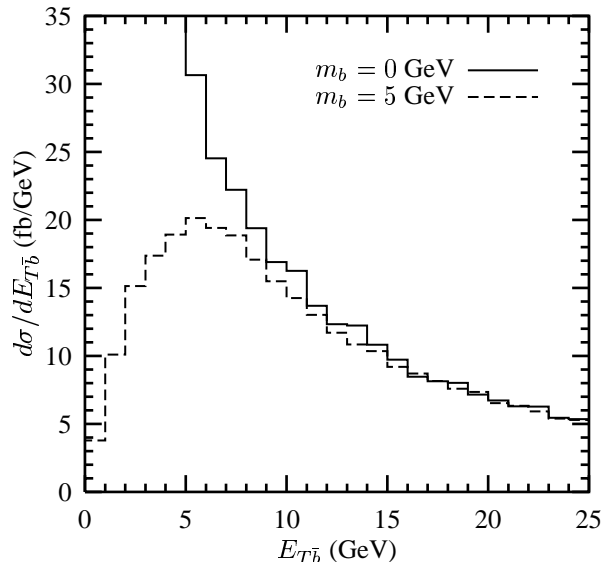


FIG. 20: Effect of the  $b$ -quark mass on the  $\bar{b}$ -jet transverse energy  $E_{T\bar{b}}$  distribution for  $t\bar{b}j$  production with no cuts.

A more realistic comparison is to consider the difference in jet distributions after cuts. The  $\bar{b}$  jet with and without the bottom-quark mass included is presented in Figs. 21 and 22, where a minimal set of cuts for potentially observable jets is defined to have  $p_{Tj} > 5$  GeV, and  $|\eta_j| < 4$ . In this more realistic case, there is very little difference between including the bottom quark mass or not. In any situation where the  $b$ -jets are expected to be taggable, the  $b$ -quark mass will have less than a 1% effect on the measured distributions.

In the  $s$ -channel cross section, the extra bottom jet is produced in the final state, and is protected from any singularities already at LO by its recoil against the heavy top quark.

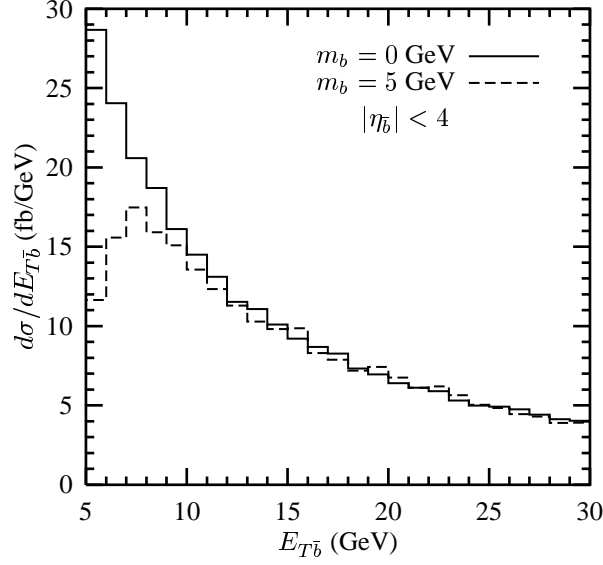


FIG. 21: Effect of the  $b$ -quark mass on the  $\bar{b}$ -jet transverse energy  $E_{T\bar{b}}$  distribution for  $t\bar{b}j$  production with cuts on both jets  $p_{Tj} > 5$  GeV and  $|\eta_j| < 4$ , and no cut on the top-quark decay products.

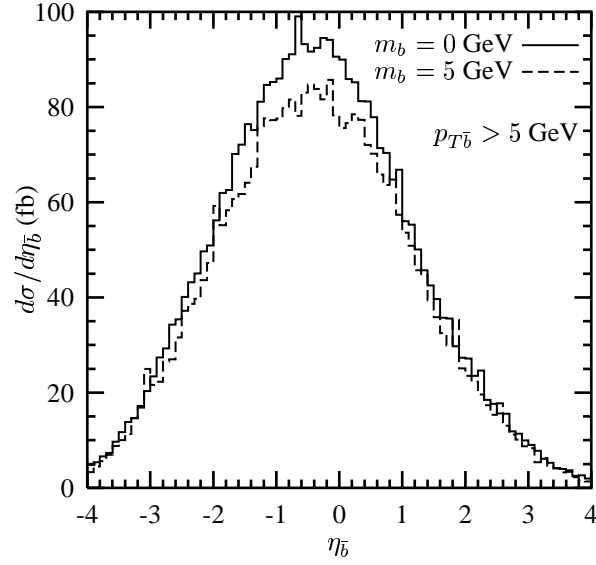


FIG. 22: Effect of the  $b$ -quark mass on the  $\bar{b}$ -jet pseudorapidity  $\eta_{\bar{b}}$  distribution for  $t\bar{b}j$  production with cuts on both jets  $p_{Tj} > 5$  GeV and  $|\eta_j| < 4$ , and no cut on the top-quark decay products.

We see in Figs. 23 and 24 that the massless and massive  $b$  distributions are already indistinguishable without any cuts. Since there is no visible effect in the measurable portion of the distributions, we have ignored the bottom-quark mass throughout. If, in the future, it

becomes desirable to measure the third jet below 10 GeV, then mass effects should be taken into account.

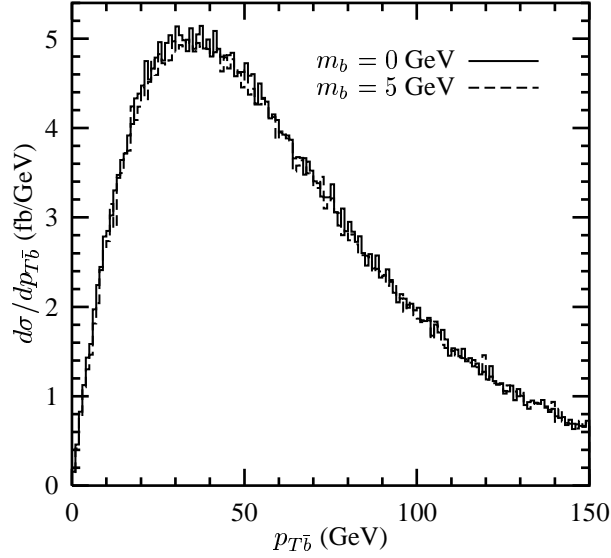


FIG. 23: Effect of the  $b$ -quark mass on the  $\bar{b}$ -jet transverse momentum distribution for  $s$ -channel single-top-quark production with no cuts.

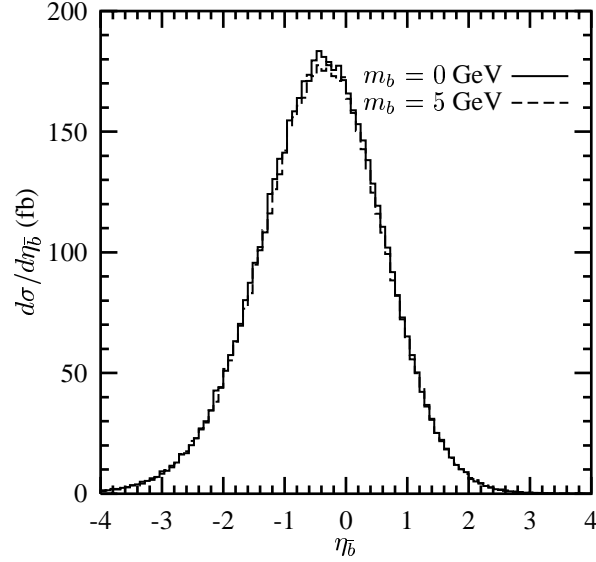


FIG. 24: Effect of the  $b$ -quark mass on the  $\bar{b}$ -jet pseudorapidity distribution for  $s$ -channel single-top-quark production with no cuts.

### III. UNCERTAINTIES

Because the measurement of  $|V_{tb}|^2$  is directly proportional to the measurement of the cross section, we must understand the uncertainties in the extracted cross section. Historically, theoretical uncertainties have been expected to dominate the cross section measurement. In particular there are two significant sources of uncertainty, the uncertainty in the quark-gluon luminosity hidden inside the  $b$  parton distribution function (PDF), and the modeling of the distributions of a third jet that would cause the event to be vetoed.

In the past, the PDF uncertainty for  $t(s)$ -channel single-top-quark production was approximated by assuming that it was the same as the gluon(quark) uncertainty. This crude approximation was shown to underestimate the uncertainty in the  $t$ -channel case by a factor of 1.5 [65]. This study uses the “Modified Tolerance Method” introduced in Refs. [45, 65, 66] and CTEQ6M PDFs [67] to provide the first complete estimation for both  $s$ -channel and  $t$ -channel processes. Results appear in Table III. The uncertainty at the LHC is much smaller than expected. This is partially attributable to the fact that we are probing the best measured region of the gluon PDFs, which in turn lowers the  $b$  uncertainty. There is also an anti-correlation in the quark- $b$  luminosity that stabilizes the calculation. A more conservative estimate would use just the  $b$  PDF uncertainty of  $^{+3}_{-4.2}\%$ . Newer CTEQ6M1 PDFs [68] harden the gluon and sea quarks at moderate fraction of proton momentum  $x$ . This gives a  $t$ -channel cross section for  $t$  production of 1.015 pb (a 2.5% increase) at the Tevatron, which is well within the current uncertainty estimate. In all cases, there is no change in the shapes of the kinematic distributions.

The shapes of all distributions at the Tevatron and LHC are completely insensitive to changes of top-quark mass within a few sigma of its currently measured value. Nevertheless, the recent average top-quark mass from run I data of  $m_t = 178.0 \pm 4.3$  GeV [69] reduces the overall normalization of the  $s$ -channel cross section for  $t$  (or  $\bar{t}$ ) production used in this paper by 7% to 0.41 pb at a 1.96 TeV  $p\bar{p}$  collider, and the  $t$ -channel cross section by 4.8% to 0.94 pb. At the LHC (a 14 TeV  $pp$  collider), the  $s$ -channel cross sections at 178 GeV are 6.17 pb and 3.85 pb, for  $t$  and  $\bar{t}$  production, respectively. The  $t$ -channel cross sections are 152.5 pb and 88.7 pb at the LHC, for  $t$  and  $\bar{t}$  production, respectively. Data from run II of the Tevatron should reduce the top-quark mass uncertainty to  $\pm 2$ –3 GeV, but it will remain the dominant theoretical uncertainty for  $s$ -channel production until  $\sim 30 \text{ fb}^{-1}$  of data are

accumulated.

The complete list of the theoretical uncertainties in the total cross sections are presented in Table III for the Tevatron and LHC. The uncertainty due to choice of scale is extensively discussed in Ref. [13], and has no effect on the shapes of the distributions. The mass of the  $b$  quark, and the error in  $\alpha_s = 0.118 \pm 0.003$ , play an insignificant role in the overall uncertainty for measurable quantities. For convenience, the NLO cross sections and their current total uncertainties are listed in Table IV using CTEQ5M1 PDFs [70].  $t$  and  $\bar{t}$  cross sections are the same at the Tevatron, but are listed separately at the LHC since it is a  $pp$  collider.

TABLE III: Uncertainties of the next-to-leading-order cross section at the Tevatron ( $p\bar{p}$ ) and LHC ( $pp$ ).

Process	$\times \delta m_t (\text{GeV})$	$\mu/2-2\mu$	PDF	$b$ mass	$\alpha_s(\delta_{\text{NLO}})$
$s$ -channel $p\bar{p}$	${}_{+2.71}^{-2.33}\%$	${}_{-5.0}^{+5.7}\%$	${}_{-3.9}^{+4.7}\%$	$< 0.5\%$	$\pm 1.4\%$
$pp$	${}_{+2.26}^{-1.97}\%$	$\pm 2\%$	${}_{-3.9}^{+3.3}\%$	$< 0.4\%$	$\pm 1.2\%$
$t$ -channel $p\bar{p}$	${}_{+1.75}^{-1.6}\%$	$\pm 4\%$	${}_{-8.1}^{+11.3}\%$	$< 1\%$	$\pm 0.01\%$
$pp$	${}_{+0.78}^{-0.73}\%$	$\pm 3\%$	${}_{-2.2}^{+1.3}\%$	$< 1\%$	$\pm 0.1\%$

Once we begin to calculate exclusive final states, there are additional uncertainties that arise from modeling the kinematic distributions. In Secs. II A and II B we saw that NLO distributions of the top quark and leading jet were similar to LO distributions including  $K$ -factors if physically motivated scales were chosen. The main uncertainty arises in how well the separation between  $t + 1$  jet and  $t + 2$  jet distributions is modeled. Since the NLO shapes of the jets are stable, the remaining uncertainty is entirely due to the cuts on the  $t + 2$  jet final states, which are only evaluated at LO.

Typical uncertainties may be derived by observing the change in the normalization of the jet distributions when the scales are varied by a factor of 2. The uncertainties for each final state depend on the exact cuts that are used. In Table V I list the uncertainties for the cuts in Table I and cross sections in Table II. I also provide the complete percentage uncertainty in parentheses, assuming  $\delta m_t = 4.3$  GeV, and the uncertainties in Table III. The uncertainty for a final state containing a top quark plus one or two jets is presented first. The subsamples containing zero or one taggable  $b$  jets are also listed.

TABLE IV: Next-to-leading-order inclusive cross sections for single-top-quark production at the Tevatron and LHC for  $m_t = 175$  GeV. Cross sections are evaluated with CTEQ5M1 PDFs, and  $M_{t\bar{b}}$  or the DDIS scales ( $\mu_l = Q^2$ ,  $\mu_h = Q^2 + m_t^2$ ), for  $s$ -channel or  $t$ -channel, respectively. Theoretical uncertainties are added in quadrature, and are based on an uncertainty in the top-quark mass of 4.3 GeV.

Process	$\sqrt{S}$	$\sigma_{\text{NLO}}$ (pb)
$s$ -channel	1.8 TeV $p\bar{p}$ ( $t$ )	0.377 $^{+0.052}_{-0.045}$
	1.96 TeV $p\bar{p}$ ( $t$ )	0.442 $^{+0.061}_{-0.053}$
	14 TeV $pp$ ( $t$ )	6.56 $^{+0.69}_{-0.63}$
	14 TeV $pp$ ( $\bar{t}$ )	4.09 $^{+0.43}_{-0.39}$
$t$ -channel	1.8 TeV $p\bar{p}$ ( $t$ )	0.73 $^{+0.10}_{-0.08}$
	1.96 TeV $p\bar{p}$ ( $t$ )	0.99 $^{+0.14}_{-0.11}$
	14 TeV $pp$ ( $t$ )	155.9 $^{+7.5}_{-7.7}$
	14 TeV $pp$ ( $\bar{t}$ )	90.7 $^{+4.3}_{-4.5}$

For  $s$ -channel production, the  $t\bar{b}$  final state is well modeled, and the uncertainty is completely dominated by the top-quark mass measurement. The kinematic uncertainty is less than 2.5%. The  $tj$  and  $t\bar{b}j$  final states are LO cross sections, and so are more sensitive to fluctuations of the additional radiation. The  $tj$  and  $t\bar{b}j$  cross sections have approximately  $^{+20}_{-16}\%$  kinematic uncertainties in their normalizations, but have very low rates, and are not necessary for observation of the signal.

In the  $t$ -channel, the uncertainty in the  $tj$  final state was previously estimated [23] to be  $\pm 15\%$ , based solely on how often the  $t\bar{b}j$  Feynman diagram produced a  $b$  jet with  $p_{Tb} < 15$  GeV. The same large logarithms that lead to the need for the introduction of a  $b$  PDF, also produce a large uncertainty in the shape and normalization of the  $b$  jet distributions. Changes in the two scales in the problem ( $Q^2$  and  $Q^2 + m_t^2$ ) tend to accidentally cancel. Therefore, an accurate estimation of uncertainty requires varying the scales independently.

The full NLO calculation tells us that the kinematic uncertainty of the jet in the  $tj$  final state is only about 6.5% if flavor is ignored. The decrease comes from two effects. First, only 2/3 of the additional radiation that is cut on includes the poorly modeled  $b$  jet distribution. Second, the addition of a cut in pseudorapidity removes the forward  $b$  jets that are missed.



TABLE V: Uncertainties in normalization of jet distributions (pb) in the  $t + n$  jet final states for  $t$  (or  $\bar{t}$ ) production at a 1.96 TeV  $p\bar{p}$  collider. These uncertainties are valid for the cuts in Table I and cross sections in Table II. Total percentage uncertainties are listed in parentheses, and include the uncertainties from Table III added in quadrature assuming  $\delta m_t = 4.3$  GeV.

Process	$j$ flavors	$t + 1$ jet	$t + 2$ jets
$t$ -channel	all	$+0.028$ $-0.036$ pb $\left(\begin{smallmatrix} +15\% \\ -13\% \end{smallmatrix}\right)$	$+0.025$ $-0.019$ pb $\left(\begin{smallmatrix} +18\% \\ -14\% \end{smallmatrix}\right)$
	0 $b$ jets	$+0.037$ $-0.048$ pb $\left(\begin{smallmatrix} +16\% \\ -15\% \end{smallmatrix}\right)$	$+0.018$ $-0.014$ pb $\left(\begin{smallmatrix} +17\% \\ -14\% \end{smallmatrix}\right)$
	1 $b$ jet	$+0.011$ $-0.009$ pb $\left(\begin{smallmatrix} +21\% \\ -16\% \end{smallmatrix}\right)$	$+0.007$ $-0.005$ pb $\left(\begin{smallmatrix} +21\% \\ -16\% \end{smallmatrix}\right)$
$s$ -channel	all	$+0.007$ $-0.009$ pb $\left(\begin{smallmatrix} +13\% \\ -11\% \end{smallmatrix}\right)$	$+0.017$ $-0.013$ pb $\left(\begin{smallmatrix} +24\% \\ -19\% \end{smallmatrix}\right)$
	1 $b$ jet	$+0.005$ $-0.007$ pb $\left(\begin{smallmatrix} +13\% \\ -11\% \end{smallmatrix}\right)$	$+0.013$ $-0.010$ pb $\left(\begin{smallmatrix} +24\% \\ -19\% \end{smallmatrix}\right)$
	0 $b$ jets	$+0.002$ $-0.002$ pb $\left(\begin{smallmatrix} +24\% \\ -19\% \end{smallmatrix}\right)$	

Hence, the kinematic uncertainty in the  $tj$  final state is smaller than either the PDF or top-quark mass uncertainties. The NLO distribution of  $tj$  when the jet does not contain a  $b$  is known to  $^{+7.7}_{-10}\%$ . This is still better than, but comparable to the PDF and top-quark mass uncertainties. If tighter cuts are made, this uncertainty will improve. Finally, the LO  $tb$  final state still has an uncertainty of about  $^{+16}_{-12}\%$ . In general, more inclusive cross sections are better estimated.

There are two remaining uncertainties that can appear in the theoretical calculation, but which are not estimated here. In Sec. IV a matching between the NLO calculation and event generators is proposed. Uncertainties arising from the normalization of the distributions produced by the event generators can only be calculated when the fits are performed. The last uncertainty comes from the fact that the top quark is not decayed in this analysis. A leading-order estimate already limits this uncertainty to less than 2% for the distributions and search strategy discussed here. However, if angular correlations are measured [23, 71], or extreme cuts are used, then this uncertainty may be enhanced. A simple remedy would be to include the decay of the top quark by combining the complete published next-to-leading-order spin-density matrices for production [13] and decay [72] into a single program.

## IV. COMPARISON TO EVENT GENERATORS

The motivation for performing differential calculations at next-to-leading order is to improve the connection between theory and experimental results. Typically, this connection is made through the use of a showering event generator. These event generators begin with leading-order matrix elements, and model the effects of soft initial and final-state showering, and hadronization. The essential question is whether these modified leading-order calculations are sufficiently predictive for the final states that will be measured. For PYTHIA [61] and HERWIG [60], the answer is a resounding no.

### A. $t$ -channel production in HERWIG and PYTHIA

We begin by examining  $t$ -channel single-top-quark production at the Tevatron (see Ref. [47] for a summary of the situation at the LHC). PYTHIA and HERWIG both produce events by evaluating the hard cross section represented by Fig. 25. Beginning with the correct LO diagram for  $t + 1$  jet production, the programs apply soft showering to the final-state quarks (which does not change the primary direction of the overall jet), and use strong-angular-ordered showering for incoming quarks. Using the cuts of Table I, we see in Figs. 26 and 27 that the extra jet is reasonably well represented if it is *not* a  $b$  jet. PYTHIA and HERWIG have been normalized to the inclusive NLO cross section (the  $K$ -factor is the same if you normalize to the  $t + 1$  jet inclusive cross section after cuts). The main discrepancy here is that PYTHIA overestimates the signal by 8%, while HERWIG underestimates it by 5%.

Unfortunately, both PYTHIA and HERWIG predict completely incorrect distributions for the  $b$  jet in the  $t+b$ -jet sample. In Fig. 28 we see that the transverse momentum predicted by the event generators is too soft. While we can imagine trying to harden the spectrum by tuning parameters of the event generator, we cannot tune the pseudorapidity distributions of Fig. 29. The showering event generators are producing  $b$  jets that are too far forward. Once central cuts are placed, PYTHIA (HERWIG) underestimates the number of events in this channel by at least a factor of 2.75 (1.4); tighter cuts produce a greater underestimate. The origin of the problem is that the showering event generators only produce additional  $b$  jets from the soft angular-ordered initial-state radiation. All jets produced this way lead to

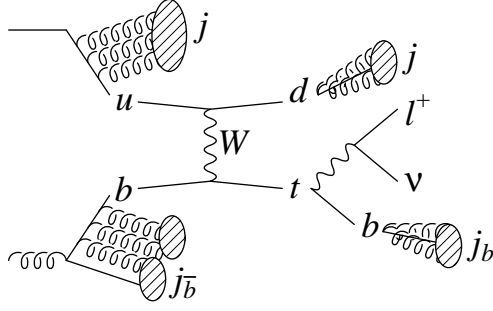


FIG. 25: A symbolic representation of  $t$ -channel single-top-quark production as generated by HERWIG and PYTHIA. Soft angular-ordered showering is applied to the hard matrix element for  $ub \rightarrow td$ . The radiation is hadronized, and resummed using a jet definition.

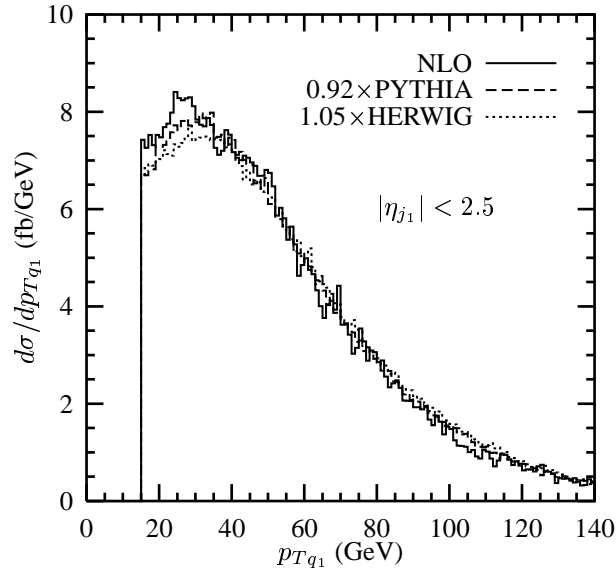


FIG. 26: Transverse momentum  $p_{Tq_1}$  of the observed non- $b$  jet in the  $t + 1$  jet final state (“jet veto”) of  $t$ -channel production from NLO (solid), PYTHIA (dashed), and HERWIG (short-dashed) normalized to NLO.

distributions that are too soft and too far forward.

The failure of PYTHIA and HERWIG to model the  $t + b$ -jet final state has several important consequences: Analyses and acceptance studies using PYTHIA or HERWIG will lead to approximately a factor of 3 underestimate of the cross section in the  $Wb\bar{b}$  bin. This means the cross section for discovery is larger than currently estimated. However, this also means that the background to other physics analyses has been severely underestimated. The obvious case is for  $s$ -channel single-top-quark production, which is distinguished from

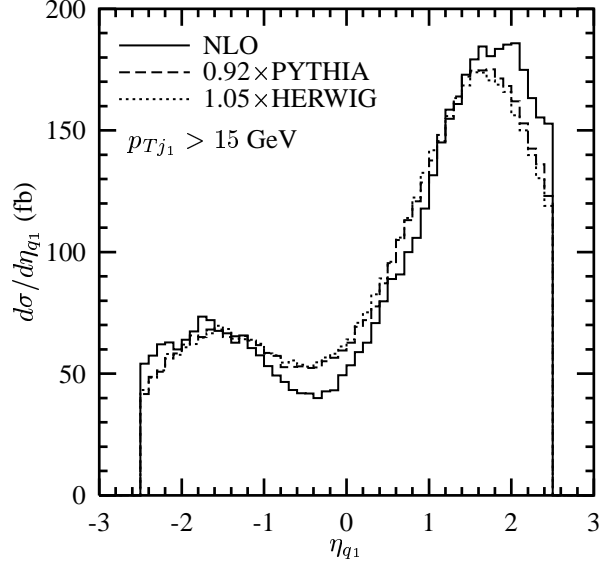


FIG. 27: Pseudorapidity  $\eta_{q_1}$  of the observed non- $b$  jet in the  $t + 1$  jet final state (“jet veto”) of  $t$ -channel production from NLO (solid), PYTHIA (dashed), and HERWIG (short-dashed) normalized to NLO.

$t$ -channel production by the number of  $b$  tags. Also, the Higgs analysis ( $WH \rightarrow Wb\bar{b}$ ) will have a significantly larger contribution from  $t$ -channel production than estimated. For lighter Higgs masses ( $< 130$  GeV) single-top-quark production may be a more significant background than  $t\bar{t}$  production.

The shapes of the distributions in the  $t + 2$ -jet final state are also not well-modeled by HERWIG and PYTHIA. In Fig. 30 we see the transverse momentum and pseudorapidities of  $b$  and non- $b$  jets scaled to the NLO event rate. The non- $b$  leading jets  $q_1$  are reasonable in shape, but either over or underestimated in rate by up to 15%. Other distributions are off in rate by up to a factor of 2, and the pseudorapidities are poorly reproduced by both HERWIG and PYTHIA. A method for correcting these samples is discussed in Sec. IV C.

### B. $s$ -channel production in HERWIG and PYTHIA

The  $s$ -channel cross section is not well represented by either HERWIG or PYTHIA. In Figs. 31–35 we see that the event generators *overestimate* the number of events in all final states that include additional radiation, and *underestimate* the number in the  $t + b$ -jet ( $Wb\bar{b}$ ) final state. The origin of this artifact in PYTHIA is that  $s$ -channel production is

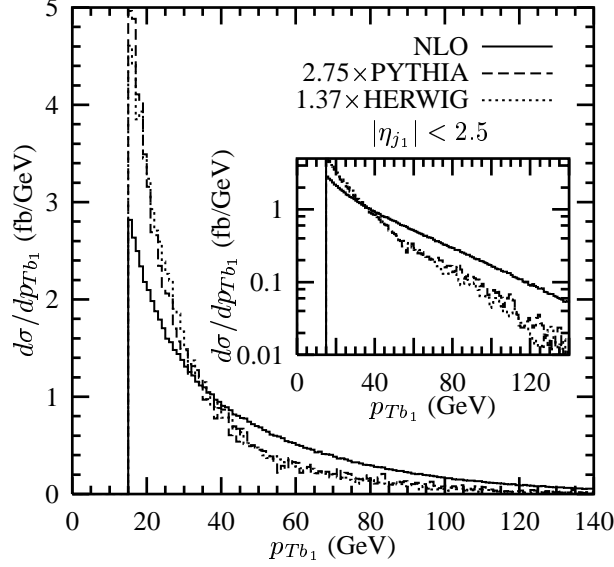


FIG. 28: Transverse momentum  $p_{Tb_1}$  of the observed  $b$  jet in the  $t+1$  jet final state (“jet veto”) of  $t$ -channel production from NLO (solid), PYTHIA (dashed), and HERWIG (short-dashed) normalized to NLO. Inset is on a logarithmic scale.

implemented by producing a  $W'$  that is set to have the same mass as a real  $W$  boson. The problem is that the scale is hard-coded to be the  $W'$  mass. Hence, this extra radiation comes from using too small a scale. The scale should be something on the order of the invariant mass of the  $t\bar{b}$  pair [13], or at least the top-quark mass. HERWIG also uses a scale that is too small, but it uses different scales in the hard cross section for different events. For example, gluon-initiated events use an average hard scale around 100 GeV, and sometimes use a hard scale less than 1 GeV. This artificially overweights those events which have additional radiation.

The shapes of the transverse momentum spectra are reasonably well modeled by both event generators, but additional radiation is too sharply peaked at small pseudorapidity. Hence, analyses with tighter cuts than shown in Figs. 31–35 will demonstrate a larger discrepancy. The net effect is that  $s$ -channel production in the  $tb$ -jet ( $Wbb$ ) final state has been underestimated by the event generators by at least a factor of 1.32–1.45; whereas in the  $t+1$  non- $b$ -jet final state, the signal is overestimated by at least a factor of 2–2.4. In the  $t+2$  jet final state, both generators overestimate the number of events by at least a factor of 1.4–2.3 depending on the exact final state. Since the discovery channel is  $Wb\bar{b}$ , it should be easier to find  $s$ -channel production than previously estimated by the experiments.

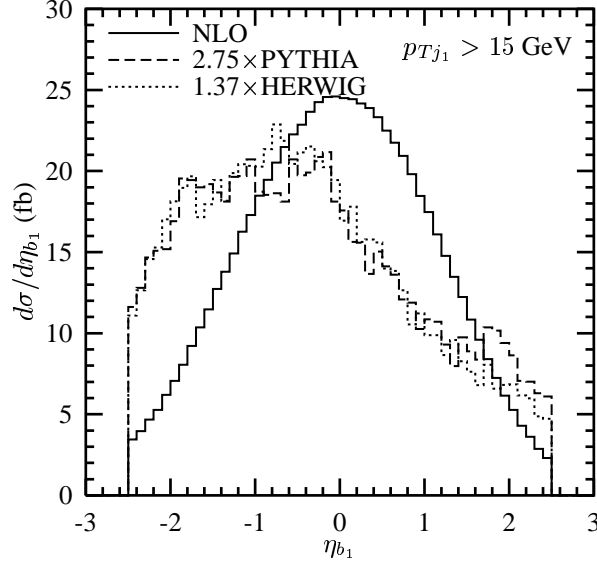


FIG. 29: Pseudorapidity  $\eta_{b_1}$  of the observed  $b$  jet  $b_1$  in the  $t + 1$  jet final state (“jet veto”) of  $t$ -channel production from NLO (solid), PYTHIA (dashed), and HERWIG (short-dashed) normalized to NLO.

However, this means that the  $s$ -channel contribution to  $Wb\bar{b}$  as a background to low-mass Higgs production has been underestimated by the same amount.

### C. Correcting the event generators

The first general-purpose next-to-leading-order showering event generators for hadron colliders are beginning to appear [73]. However, they continue to rely on the ability to cleanly separate initial-state and final-state radiation. Single-top-quark production through the  $s$ -channel exhibits such a separation, but has not yet been added to the programs. A corrected leading-order generator using a  $K$ -factor is expected to perform well enough. On the other hand, there is no clear separation in  $t$ -channel production between initial-state and final-state radiation. Given the similarity to deep-inelastic scattering, it may be possible to construct a next-to-leading-order event generator for  $t$ -channel production [74], but no working implementation exists. Nevertheless, in order to compute detector efficiencies it is necessary to have predictions at the level of detectable particles (pions, photons, etc.). Therefore, I propose a simple matching prescription that bypasses many of the problems [75].

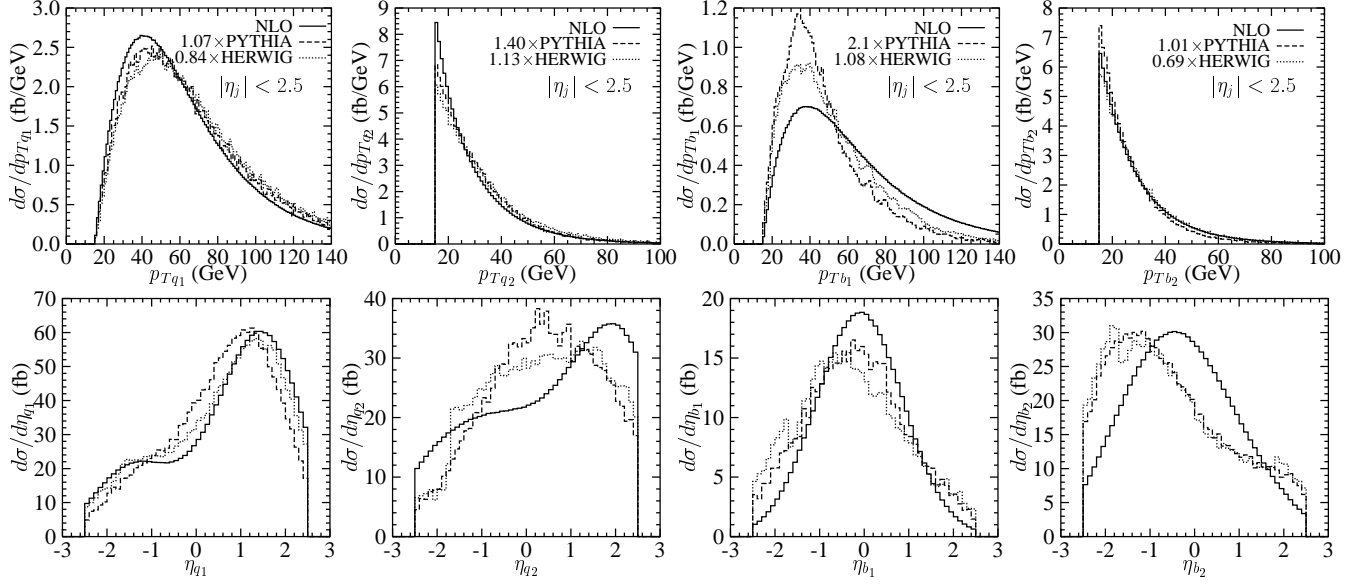


FIG. 30: Transverse momentum  $p_T$  and pseudorapidity  $\eta$  for the  $p_T$ -ordered jets  $j_i$  in the  $t + 2$ -jet final state of  $t$ -channel production from NLO (solid), PYTHIA (dashed), and HERWIG (short-dashed).  $j_1$  and  $j_2$  are divided into non- $b$  jets  $q_i$  and  $b$  jets  $b_i$ . Curves are normalized to NLO in each column.

The goal is to produce a set of events with the proper shape and normalization. The most important thing to match is the shape of the distributions in a given final state. Once the shapes are matched, generated events may be multiplied by an overall probability that is normalized by the NLO calculations after cuts. This prescription is based on the essential understanding that the next-to-leading-order calculations are jet calculations. Therefore, matching must be done at the jet level. This is accomplished in four steps.

1. Generate events with MadEvent [76] or CompHEP [77] using the tree-level Feynman diagrams that produce all measurable final states. The  $t$ -channel parton-level processes for top-quark production are  $qb \rightarrow tq'$ ,  $qb \rightarrow tq'g$ ,  $gb \rightarrow t\bar{q}q'$ , and  $qg \rightarrow tq'\bar{b}$ , where  $q$  and  $q'$  stand for the five light quarks. The  $s$ -channel parton-level processes are  $q\bar{q}' \rightarrow t\bar{b}$ ,  $q\bar{q}' \rightarrow t\bar{b}g$ ,  $qg \rightarrow t\bar{b}q'$ , and  $g\bar{q}' \rightarrow t\bar{b}\bar{q}$ . Use the DDIS scales ( $\mu_l = Q^2$ ,  $\mu_h = Q^2 + m_t^2$ ) for  $t$ -channel production, and  $M_{t\bar{b}}$  for  $s$ -channel production to minimize changes in the shape between LO and NLO.
2. Feed these events into HERWIG or PYTHIA with full showering turned on.
3. Create four samples ( $tj$ ,  $t\bar{b}$ ,  $tjj$ , and  $t\bar{b}j$ ) for  $t$ -channel production with minimal cuts,

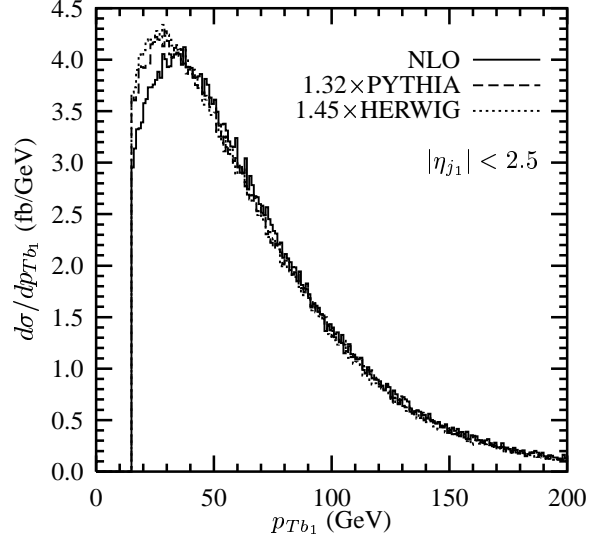


FIG. 31: Transverse momentum  $p_{Tb_1}$  of the observed  $b$  jet in the  $t+1$  jet final state (“jet veto”) of  $s$ -channel production from NLO (solid), PYTHIA (dashed), and HERWIG (short-dashed) normalized to NLO.

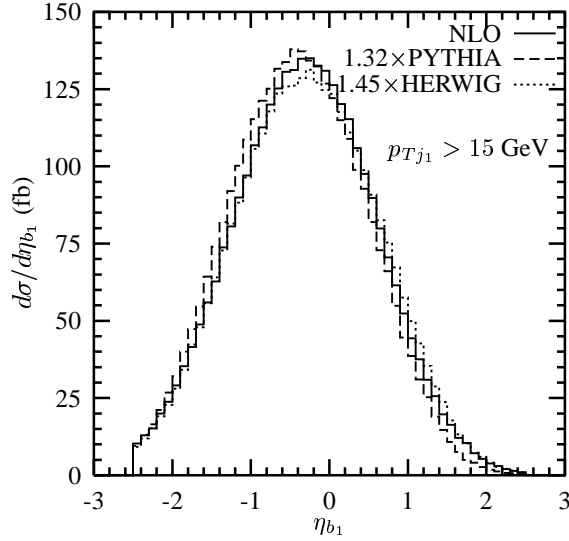


FIG. 32: Pseudorapidity  $\eta_{b_1}$  of the observed  $b$  jet  $b_1$  in the  $t+1$  jet final state (“jet veto”) of  $s$ -channel production from NLO (solid), PYTHIA (dashed), and HERWIG (short-dashed) normalized to NLO.

and a well-defined jet definition, e.g.,  $k_T$  clustering with  $\Delta R < 1$ , applied to stable particles in the event record ( $\pi^\pm$ ,  $\gamma$ ,  $e^\pm$ ,  $\mu^\pm$ , etc.).  $s$ -channel production will have three samples ( $tb$ ,  $tj$ , and  $tbj$ ).



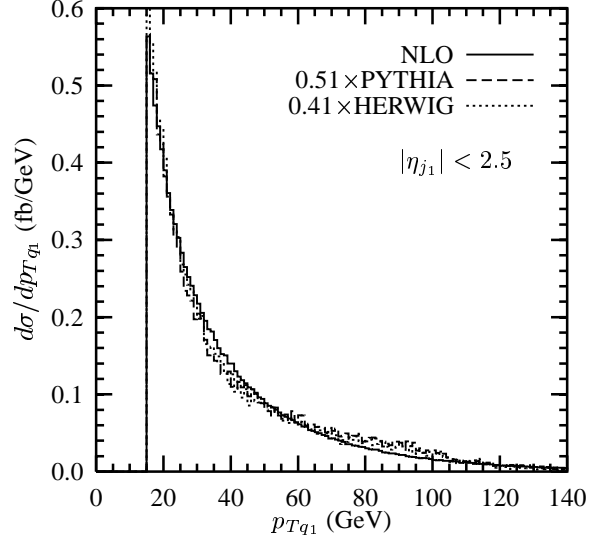


FIG. 33: Transverse momentum  $p_{Tq_1}$  of the observed non- $b$  jet in the  $t + 1$  jet final state (“jet veto”) of  $s$ -channel production from NLO (solid), PYTHIA (dashed), and HERWIG (short-dashed) normalized to NLO.

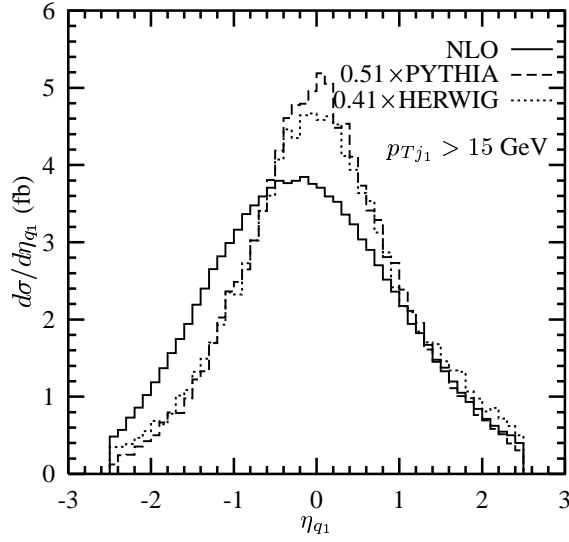


FIG. 34: Pseudorapidity  $\eta_{q_1}$  of the observed non- $b$  jet in the  $t + 1$  jet final state (“jet veto”) of  $s$ -channel production from NLO (solid), PYTHIA (dashed), and HERWIG (short-dashed) normalized to NLO.

4. Produce the same final states with the NLO calculation, and use the same cuts and jet definition. Normalize the weights of the events in each of the event generator samples to the cross sections of these NLO samples. Remember that the NLO jets should be

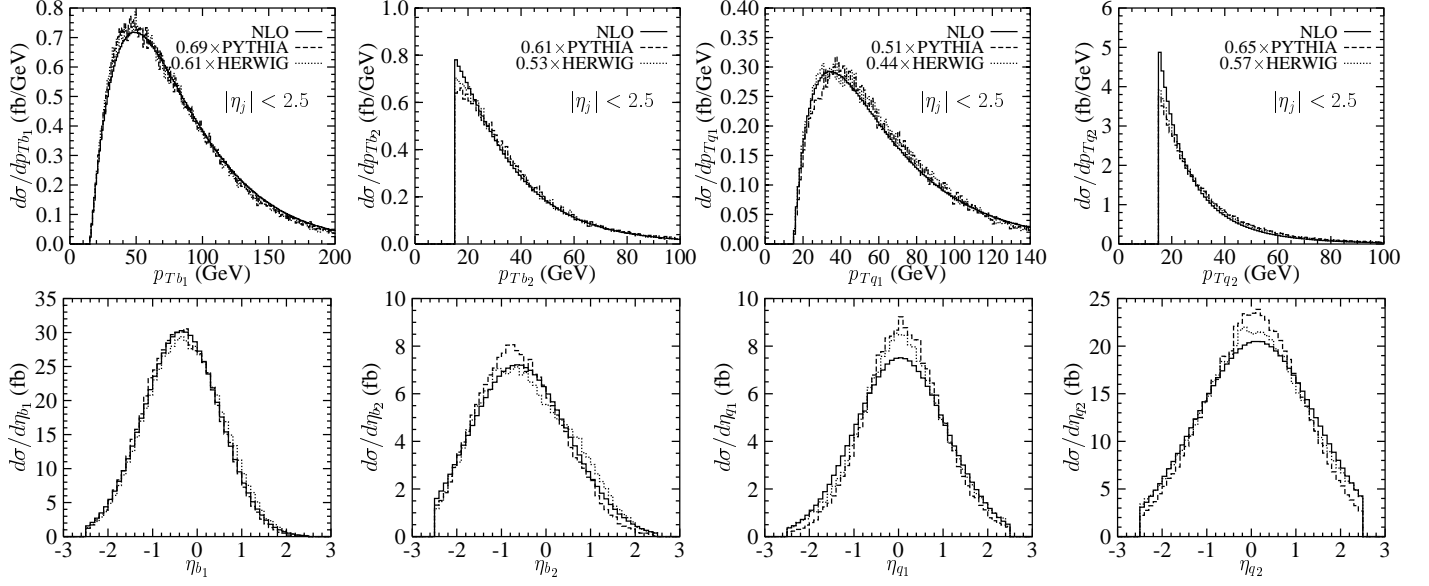


FIG. 35: Transverse momentum  $p_T$  and pseudorapidity  $\eta$  for the  $p_T$ -ordered jets  $j_i$  in the  $t + 2$ -jet final state of  $s$ -channel production from NLO (solid), PYTHIA (dashed), and HERWIG (short-dashed).  $j_1$  and  $j_2$  are divided into  $b$  jets  $b_i$  and non- $b$  jets  $q_i$ . Curves are normalized to NLO in each column.

$E_T$ -ordered, but that explicit heavy-flavors in the final state must be tracked.

In principle we would want to apply the jet definition to the event generators at the point of clustering. However, this is not possible in PYTHIA because of the order in which events are processed. Furthermore, both event generators do some slight reshuffling and energy rebalancing at a later point in the process. The NLO calculation is not aware of long-range final-state effects, but constraints in the event generators on the direction of particles coming from the clustering stage maintain the correspondence with the perturbative calculation. Matching to jets produced out of stable particles has been found to work to better than 1% (the limit of the statistical accuracy checked) for the simpler case of  $s$ -channel  $W'$  production [45, 47], where the event generators perform well. In general, a systematic study of the uncertainty in the matching should be performed for each set of cuts.

## V. CONCLUSIONS

Precise measurements of single-top-quark production in both the  $s$ -channel and  $t$ -channel modes will begin to appear within the next few years using data from run II of the Fermilab

Tevatron, and eventually the CERN LHC. These cross sections are distinguished by the frequency of  $b$  jets occurring in the  $W + 2$  jet sample, with  $Wb\bar{b}$  ( $Wbj$ ) most often coming from  $s$ -( $t$ -)channel production. These measurements will provide direct extraction of the CKM matrix element  $V_{tb}$ , and may allow discovery and interpretation of new physics.

Historically, the ability to interpret the measurement of the single-top-quark cross sections was expected to be dominated by theoretical uncertainties. In Sec. III, we see that these uncertainties, while still large, are under much better control. The uncertainty in the top-quark mass completely dominates the prediction for the  $s$ -channel cross section, but this will improve with additional data. The measurement of the  $s$ -channel cross section will be statistics limited at the Tevatron, and difficult to distinguish from backgrounds at the LHC [23]. Hence, the theoretical uncertainty in  $s$ -channel production should be smaller than the expected experimental accuracy at either a high-luminosity Tevatron, or the LHC.

Current theoretical uncertainties in  $t$ -channel production limit extraction of  $V_{tb}$  to about  $\pm 8\%$ . The next-to-leading-order distributions presented in Secs. II A and IV A improve the kinematic uncertainty in  $t$ -channel production, so that parton distribution function uncertainties will dominate our ability to interpret the data. This uncertainty could be reduced by measuring the ratio of  $t$ -channel production to  $Zb$  production. However, the latter cross section is small, and thus we should consider alternate possibilities, such as  $Wc$  or  $Wj$  exclusive final states. Any improvement in the measurement of the  $b$  or gluon distributions at scales near the top-quark mass, and proton momentum fraction  $x$  near 0.1, will directly reduce the remaining theoretical uncertainty.

The availability of fully differential next-to-leading-order calculations for hadronic processes has begun a new era of precision comparisons between theory and experiment. In order to fully realize the potential of these theoretical improvements, we must first understand how to interpret the calculations. In Sec. II, we see that NLO calculations produce *jet* distributions in the final state, rather than *parton* distributions. This forces us to describe the results in terms of  $E_T$ -ordered jets, rather than NLO distributions of a specific quark. It further ties the theoretical results to the explicit choice of jet definition. We see in Sec. II C that the effect of jet definition on the shapes of distributions is larger than all theoretical uncertainties combined.

Finally, fixed-order calculations are generally compared to showering event generators, such as PYTHIA and HERWIG, rather than directly to data, in order to understand detector

efficiencies. Therefore, we must understand how to compare next-to-leading-order jets to jets produced from showering. A simple matching scheme is presented in Sec. IV C, that uses the NLO calculation to normalize the measurable event samples. Ultimately, we would like to have a next-to-leading-order event generator that can handle initial-state and final-state interferences.

Now that the theoretical predictions for single-top-quark production are under control, a few questions remain regarding the decay of the top quark. One of the most interesting features of single-top-quark production is the possibility of measuring the polarization of the top quark [23, 71, 72]. The program used to produce distributions for this paper, ZTOP, does not decay the top quark. However the complete analytic NLO spin-density matrices for production do appear in Ref. [13], and could be combined with the known NLO decays from Ref. [72].

A spin-dependent program would allow an estimate of the uncertainties associated with using alternate search strategies, such as cutting on  $H_T$ , the scalar sum of the transverse energies of the particles in the event. It is clear from the distributions in Sec. IV, that the  $H_T$  for single-top-quark production is larger than predicted at LO in the  $W + 2$  jet inclusive sample. The inclusion of top-quark decay is necessary to determine whether this is a serious problem or not. Ultimately, a program that includes decays will be necessary to determine whether the single-top-quark background to new physics, such as Higgs production, has been greatly underestimated, or whether specific cuts accidentally reduce the discrepancies. For now, however, we have a reliable theoretical calculation, and method for matching to event generators, that will allow for accurate interpretation of single-top-quark production data when it is discovered.

## Acknowledgments

This work is supported by the U.S. Department of Energy, High Energy Physics Division, under contract DE-AC02-76CH03000.

---

[1] CDF Collaboration, A. Juste, hep-ex/0406041.

- [2] CDF Collaboration, C. I. Ciobanu, Int. J. Mod. Phys. A **16S1A**, 389 (2001); CDF Collaboration, D. Acosta *et al.*, Phys. Rev. D **65**, 091102 (2002); CDF Collaboration, T. Kikuchi, S. K. Wolinski, L. Demortier, S. Kim, and P. Savard, Int. J. Mod. Phys. A **16S1A**, 382 (2001); CDF Collaboration, D. Acosta *et al.*, Phys. Rev. D **69**, 052003 (2004).
- [3] D0 Collaboration, V. M. Abazov *et al.*, Phys. Lett. B **517**, 282 (2001); D0 Collaboration, B. Abbott *et al.*, Phys. Rev. D **63**, 031101 (2001); D0 Collaboration, A. P. Heinson, Int. J. Mod. Phys. A **16S1A**, 386 (2001).
- [4] *Report of the tev\_2000 Study Group*, edited by D. Amidei and R. Brock, Fermilab-Pub-96/082 (1996).
- [5] M. Beneke *et al.*, in *Proceedings of the Workshop on Standard Model Physics (and More) at the LHC*, edited by G. Altarelli, and M. L. Mangano (CERN, Geneva, 2000), p. 456, hep-ph/0003033.
- [6] S. S. Willenbrock and D. A. Dicus, Phys. Rev. D **34**, 155 (1986).
- [7] C. P. Yuan, Phys. Rev. D **41**, 42 (1990).
- [8] R. K. Ellis and S. Parke, Phys. Rev. D **46**, 3785 (1992).
- [9] D. O. Carlson and C. P. Yuan, Phys. Lett. B **306**, 386 (1993).
- [10] A. P. Heinson, A. S. Belyaev, and E. E. Boos, Phys. Rev. D **56**, 3114 (1997).
- [11] G. Bordes and B. van Eijk, Nucl. Phys. B **435**, 23 (1995).
- [12] T. Stelzer, Z. Sullivan, and S. Willenbrock, Phys. Rev. D **56**, 5919 (1997).
- [13] B. W. Harris, E. Laenen, L. Phaf, Z. Sullivan, and S. Weinzierl, Phys. Rev. D **66**, 054024 (2002).
- [14] S. Cortese and R. Petronzio, Phys. Lett. B **253**, 494 (1991).
- [15] T. Stelzer and S. Willenbrock, Phys. Lett. B **357**, 125 (1995).
- [16] M. C. Smith and S. Willenbrock, Phys. Rev. D **54**, 6696 (1996).
- [17] S. Mrenna and C. P. Yuan, Phys. Lett. B **416**, 200 (1998).
- [18] B. W. Harris, E. Laenen, L. Phaf, Z. Sullivan, and S. Weinzierl, Int. J. Mod. Phys. A **16S1A**, 379 (2001).
- [19] T. M. P. Tait, Phys. Rev. D **61**, 034001 (2000).
- [20] A. Belyaev and E. Boos, Phys. Rev. D **63**, 034012 (2001).
- [21] S. Moretti, Phys. Rev. D **56**, 7427 (1997).
- [22] S. Zhu, hep-ph/0109269.

- [23] T. Stelzer, Z. Sullivan, and S. Willenbrock, Phys. Rev. D **58**, 094021 (1998).
- [24] T. Tait and C. P. Yuan, Phys. Rev. D **63**, 014018 (2001); hep-ph/9710372.
- [25] D. O. Carlson, E. Malkawi, and C. P. Yuan, Phys. Lett. B **337**, 145 (1994).
- [26] G. L. Kane, G. A. Ladinsky, and C. P. Yuan, Phys. Rev. D **45**, 124 (1992).
- [27] T. G. Rizzo, Phys. Rev. D **53**, 6218 (1996).
- [28] T. Tait and C. P. Yuan, Phys. Rev. D **55**, 7300 (1997).
- [29] A. Datta and X. Zhang, Phys. Rev. D **55**, 2530 (1997).
- [30] K. Whisnant, J. M. Yang, B. L. Young, and X. Zhang, Phys. Rev. D **56**, 467 (1997).
- [31] E. Boos, L. Dudko, and T. Ohl, Eur. Phys. J. C **11**, 473 (1999).
- [32] D. Espriu and J. Manzano, Phys. Rev. D **65**, 073005 (2002).
- [33] T. Han, M. Hosch, K. Whisnant, B. L. Young, and X. Zhang, Phys. Rev. D **58**, 073008 (1998).
- [34] E. H. Simmons, Phys. Rev. D **55**, 5494 (1997).
- [35] G. Lu, Y. Cao, J. Huang, J. Zhang, and Z. Xiao, hep-ph/9701406.
- [36] P. Baringer, P. Jain, D. W. McKay, and L. L. Smith, Phys. Rev. D **56**, 2914 (1997).
- [37] C. X. Yue and G. R. Lu, Chin. Phys. Lett. **15**, 631 (1998).
- [38] C. X. Yue, Y. P. Kuang, and G. R. Lu, Phys. Rev. D **56**, 291 (1997).
- [39] H. J. He and C. P. Yuan, Phys. Rev. Lett. **83**, 28 (1999).
- [40] J. j. Cao, Z. h. Xiong, and J. M. Yang, Phys. Rev. D **67**, 071701 (2003).
- [41] A. Datta, P. J. O'Donnell, Z. H. Lin, X. Zhang, and T. Huang, Phys. Lett. B **483**, 203 (2000).
- [42] X. Li and E. Ma, Phys. Rev. Lett. **47**, 1788 (1981).
- [43] E. Malkawi, T. Tait, and C. P. Yuan, Phys. Lett. B **385**, 304 (1996).
- [44] D. J. Muller and S. Nandi, Phys. Lett. B **383**, 345 (1996).
- [45] Z. Sullivan, Phys. Rev. D **66**, 075011 (2002).
- [46] CDF Collaboration, D. Acosta *et al.*, Phys. Rev. Lett. **90**, 081802 (2003).
- [47] Zack Sullivan, “How to rule out Little Higgs (and constrain many other models) at the LHC,” to be published in *Proceedings of the XXXVIIIth Rencontres de Moriond: QCD and High Energy Hadronic Interactions*, Les Arcs, Savoie, France, March 22–29, 2003, hep-ph/0306266.
- [48] D. Atwood, S. Bar-Shalom, G. Eilam, and A. Soni, Phys. Rev. D **54**, 5412 (1996).
- [49] S. Bar-Shalom, D. Atwood, and A. Soni, Phys. Rev. D **57**, 1495 (1998).
- [50] E. Christova, S. Fichtinger, S. Kraml, and W. Majerotto, Phys. Rev. D **65**, 094002 (2002).
- [51] C. S. Li, R. J. Oakes, and J. M. Yang, Phys. Rev. D **55**, 1672 (1997); Phys. Rev. D **55**, 5780

- (1997); C. S. Li, R. J. Oakes, J. M. Yang, and H. Y. Zhou, Phys. Rev. D **57**, 2009 (1998).
- [52] A. Datta, J. M. Yang, B. L. Young, and X. Zhang, Phys. Rev. D **56**, 3107 (1997).
  - [53] R. J. Oakes, K. Whisnant, J. M. Yang, B. L. Young, and X. Zhang, Phys. Rev. D **57**, 534 (1998).
  - [54] K. i. Hikasa, J. M. Yang, and B. L. Young, Phys. Rev. D **60**, 114041 (1999).
  - [55] P. Chiappetta, A. Deandrea, E. Nagy, S. Negroni, G. Polesello, and J. M. Virey, Phys. Rev. D **61**, 115008 (2000).
  - [56] *R*-parity Working Group Collaboration, B. Allanach *et al.*, in *Physics at Run II: the Supersymmetry/Higgs Workshop*, Fermilab, 1998, edited by M. Carena and J. Lykken (Fermilab, Batavia, 2002), p. 299, hep-ph/9906224.
  - [57] Higgs Working Group Collaboration, M. Carena *et al.*, in *Physics at Run II: the Supersymmetry/Higgs Workshop*, Fermilab, 1998, edited by M. Carena and J. Lykken (Fermilab, Batavia, 2002), p. 424, hep-ph/0010338.
  - [58] SUGRA Working Group Collaboration, S. Abel *et al.*, in *Physics at Run II: the Supersymmetry/Higgs Workshop*, Fermilab, 1998, edited by M. Carena and J. Lykken (Fermilab, Batavia, 2002), p. 70, hep-ph/0003154.
  - [59] E. L. Berger, B. W. Harris, and Z. Sullivan, Phys. Rev. Lett. **83**, 4472 (1999); Phys. Rev. D **63**, 115001 (2001).
  - [60] G. Corcella *et al.*, J. High Energy Phys. **01**, 010 (2001).
  - [61] T. Sjöstrand *et al.*, Comput. Phys. Commun. **135**, 238 (2001).
  - [62] A. S. Belyaev, E. E. Boos, and L. V. Dudko, Phys. Rev. D **59**, 075001 (1999).
  - [63] M. Dittmar, F. Pauss, and D. Zurcher, Phys. Rev. D **56**, 7284 (1997).
  - [64] S. D. Ellis and D. E. Soper, Phys. Rev. D **48**, 3160 (1993).
  - [65] Z. Sullivan and P. M. Nadolsky, in *Proceedings of Snowmass 2001: the Future of Particle Physics*, edited by N. Graf (Stanford Linear Accelerator Center, Stanford, 2002), eConf C010630, P511, hep-ph/0111358.
  - [66] P. M. Nadolsky and Z. Sullivan, in *Proceedings of Snowmass 2001: the Future of Particle Physics*, edited by N. Graf (Stanford Linear Accelerator Center, Stanford, 2002), eConf C010630, P510, hep-ph/0110378.
  - [67] J. Pumplin, D. R. Stump, J. Huston, H. L. Lai, P. Nadolsky, and W. K. Tung, J. High Energy Phys. **07**, 012 (2002).

- [68] D. Stump, J. Huston, J. Pumplin, W. K. Tung, H. L. Lai, S. Kuhlmann, and J. F. Owens, J. High Energy Phys. **10**, 046 (2003).
- [69] CDF Collaboration, P. Azzi *et al.*, hep-ex/0404010.
- [70] CTEQ Collaboration, H. L. Lai *et al.*, Eur. Phys. J. C **12**, 375 (2000).
- [71] G. Mahlon and S. Parke, Phys. Rev. D **55**, 7249 (1997); Phys. Lett. B **476**, 323 (2000).
- [72] A. Czarnecki, M. Jezabek, and J. H. Kuhn, Nucl. Phys. B **351**, 70 (1991); M. Fischer, S. Groote, J. G. Korner, and M. C. Mauser, Phys. Rev. D **65**, 054036 (2002); A. Brandenburg, Z. G. Si, and P. Uwer, Phys. Lett. B **539**, 235 (2002).
- [73] S. Frixione and B. R. Webber, J. High Energy Phys. **06**, 029 (2002); S. Frixione, P. Nason, and B. R. Webber, J. High Energy Phys. **08**, 007 (2003).
- [74] J. C. Collins, J. High Energy Phys. **05**, 004 (2000); J. C. Collins and F. Hautmann, J. High Energy Phys. **03**, 016 (2001); J. Collins, Phys. Rev. D **65**, 094016 (2002).
- [75] First presented by Zack Sullivan in the “The Dangerous Beauty of Single-Top-Quark Production” at the University of Chicago, November 25, 2002.
- [76] F. Maltoni and T. Stelzer, J. High Energy Phys. **02**, 027 (2003).
- [77] CompHEP Collaboration, E. Boos *et al.*, hep-ph/0403113; A. S. Belyaev *et al.*, hep-ph/0101232; E. E. Boos *et al.*, MGU-89-63/140.